A Hardware Platform for Communication and Localization Performance Evaluation of Devices inside the Human Body

by

Shen Li

A Thesis Submitted to the Faculty

of the

WORCESTER POLYTECHNIC INSTITUTE

in partial fulfillment of the requirements for the

Degree of Master of Science

in

Electrical and Computer Engineering

May 2012

APPROVED:

_____	_____
Prof. Kaveh Pahlavan, Thesis Advisor	Prof. Fred J. Looft, Department Head
_____	_____
Prof. Allen Levesque, Thesis Committee	Prof. Xinming Huang, Thesis Committee

Abstract

Body area networks (BAN) is a technology gaining widespread attention for application in medical examination, monitoring and emergency therapy. The basic concept of BAN is monitoring a set of sensors on or inside the human body which enable transfer of vital parameters between the patient´s location and the physician in charge. As body area network has certain characteristics, which impose new demands on performance evaluation of systems for communication and localization for medical sensors. However, real-time performance evaluation and localization in wireless body area networks is extremely challenging due to the unfeasibility of experimenting with actual devices inside the human body. Thus, we see a need for a real-time hardware platform, and this thesis addressed this need.

In this thesis, we introduced a unique hardware platform for performance evaluation of body area communication and in-body localization. This hardware platform utilizes a wideband multipath channel simulator, the Elektrobit PROPSim™ C8, and a typical medical implantable device, the Zarlink ZL70101 Advanced Development Kit. For simulation of BAN channels, we adopt the channel model defined for the Medical Implant Communication Service (MICS) band. Packet Reception Rate (PRR) is analyzed as the criteria to evaluate the performance of communication. Several body area propagation scenarios simulated using this hardware platform are validated, compared and analyzed. We show that among three modulations, two forms of 2FSK and 4FSK. The one with lowest raw data rate achieves best PRR, in other word, best communication performance. We also show that the channel model inside the human body predicts better communication performance than through the human body.

For in-body localization, we focus on a Received Signal Strength (RSS) based localization algorithm. An improved maximum likelihood algorithm is introduced and applied. A number of points along the propagation path in the small intestine are studied and compared. Localization error is analyzed for different sensor positions. We also compared our error result with the Cramér–Rao lower bound (CRLB), shows that our localization algorithm has acceptable performance. We evaluate multiple medical sensors as device under test with our hardware platform, yielding satisfactory localization performance.

Acknowledgements

First and foremost, I would like to express my deepest thankfulness to Professor Kaveh Pahlavan, for all the knowledge he has taught me as well as the wisdom of life he endowed on me over the two years. Without his enlightening instruction, impressive kindness and patience, I could not have accomplished my thesis.

I shall extend my thanks to my committee members, Professor Fred Looft, Professor Allen Levesque, and Professor Xinming Huang for their invaluable assistance, valuable comments and reviewing of this thesis.

I would like to express my gratitude to all colleagues in CWINS lab, especially Jie He, for his patience and valuable guidance in every stage of the writing of this thesis. He has been more than a colleague, but a co-advisor to me. I owe much of my thesis to him.

Last but not least, I must thank my beloved parents for supporting and providing me encouragement during my study abroad. Their love was the ultimate motivation in my life.

Table of Contents

List of Figures

List of Tabes

Glossary

2FSK	2 Frequency Shift Keying
4FSK	4 Frequency Shift Keying
BAN	Body Area Networks
CCA	Clear Channel Assessment
CWINS	Center for Wireless Information Network Studies
DUT	Device under Test
FDTD	Finite-difference Time-domain
HFSS	High Frequency Structure Simulator
LOS	Line of Sight
MICS	Medical Implant Communication Service
MIMO	Multiple Input Multiple Output
MLE	Maximum-Likelihood Estimation
NIST	National Institute of Standards and Technology
NLOS	Non Line of Sight
PRR	Packet Reception Rate
RSS	Receive Signal Strength
RSSI	Receive Signal Strength Indicator
RX	Receiver
TOA	Time of Arrival

TX	Transmitter
UI	User Interface
WLAN	Wireless Local Area Network
WPI	Worcester Polytechnic Institute

Chapter 1: Introduction

This chapter is divided into four sections. Section 1.1 gives some background knowledge and literature search of this hardware platform and Section 1.2 discussed the motivation of writing this thesis. In Section 1.3 gives the major contributions of this thesis and Section 1.4, the thesis outline is provided.

1.1 Background

The ongoing development of Body Area Networks (BANs) in conjunction with advances in implantable medical devices is generating great interest in use of this interdisciplinary technology for improved health care, including patient monitoring, diagnostic procedures, and emergency treatment. [1] [2] However, the development of these applications has been hampered by the technical difficulties encountered in wireless transmission through and inside the human body. Prior research shows that signal propagation through and within the body is influenced by many factors, including differing dielectric properties of various organs, body shape. From paper [3], their result shows even the effect of body shape and gender on Wireless Body Area Network on-body channel. Consequently, knowing how signals propagate through and inside the body is challenging. So far, there is no widely-accepted model for wireless propagation in the human body, though various studies have been made for localization and communication applications, such as [4] [5].

Several simulation software tools were developed for BANs communication purposes. Although these tools, e.g. HFSS from Ansoft Corporation [6] and FDTD simulated in MATLAB [7], are very useful for accurately implementing channel models for signal propagation inside the

human body, these software tools' limitations is they cannot be put to use for connecting real-world medical devices, which are necessary prerequisites to real-world field measurement. For such purposes, we have developed a real-time emulation hardware platform. For the device under test (DUT) we chose the Zarlink ZL70101 Application Development Kit (ADK), and for multipath channel emulation we chose the Elektrobit PROPSim C8 system [8], which provides a repeatable, controllable body area propagation environment. Previous work on indoor communication and localization performance testbed using the PROPSim C8 is discussed in [9] [10], [11] and [12].

In Leon T. Metreaud's master thesis [13], a real-time performance evaluation testbed for wireless local area networks (WLAN) is introduced. Azimuth™ Systems 801W was used to provide isolated environment and capture packets by a software protocol analyzer, Wild Packets Airopeek NX. Elektrobit PROPSim™ C8 multipath channel simulator was used to provide a controllable, repeatable WLAN propagation environment. Statistical data characterizing performance such as data rate and Received Signal Strength (RSS), were collected. Metreaud analyzed average throughput and instantaneous throughput variation using different channels models developed under IEEE 802.11 b and 802.11g standardization activities.

Mohammad Heidari [14] provided a testbed for performance evaluation of indoor geolocation systems. Heidari focused on the Received Signal Strength (RSS) based localization method along with fingerprinting for indoor environments. The Ekahau™ indoor positioning engine was used for performance evaluation, while the Elektrobit PROPSim™ C8 served as channel model simulator. Comparison between the simulated results of the performance evaluation of the positioning engine and the real-time performance evaluation of the

positioning system is analyzed in this thesis. Primitive error in terms of distance error is also performed.

Another Master's thesis from Muhammad Ali Assad [15] discussed a testbed for evaluating localization performance of WiFi RFID technology. That testbed consisted of Elektrobit PROPSim™ C8 RF channel simulator for multipath characteristics, several WiFi 802.11 access points, and commercial RFID tags. Assad compared the performance of the modified IEEE 802.11 channel model and the Ray Tracing channel model. Ray tracing software was also been used to evaluate the performance of two different WiFi RFID devices.

Reference [16] used Ray tracing and Elektrobit PROPSim™ C8 to simulate multipath effect for time of arrival (TOA) based indoor geolocation. This reference discussed different indoor environment scenario such as line-of-sight (LOS) and non-line-of-sight (NLOS) detectable direct path (DDP) and undetectable direct path (UDP), since the direct path being the most important for TOA-based localization method. A Trilateral-Centroid localization algorithm is proposed and used in this contribution, and many field test and simulation results are compared for both ranging error and localization error for four different scenarios. The testbed results and field test results show excellent agreement.

With future study, our work can be extended into a cyber-physical system. Cyber-Physical Systems (CPS) is integrations of computation and physical processes. Embedded computers and networks monitor and control the physical processes, usually with feedback loops where physical processes affect computations and vice versa. [17] This term refers to a new generation of systems with integrated computational and physical capabilities that can interact with humans through many new modalities. [18] Unlike most traditional embedded systems, a full-fledged CPS is typically designed as a network of interacting elements with

physical input and output instead of as standalone devices, which the ability to interact with the physical world through computation, communication, and control is crucial for future technology developments. Starting in late 2006, the US National Science Foundation (NSF) and other United States federal agencies sponsored several workshops on cyber-physical systems. [19] [20] [21] The NSF has identified cyber-physical systems as a key area of research.

In BANs, link quality can be affected by many factors, including transmission power, packet size, maximum retransmission times, signal modulation scheme, and so on. In this thesis, by using the NIST path loss models, we created a hardware platform is that can be repeated and expanded on by others. We focus on the impact of the choice of modulation scheme on link quality, by calculating packet reception rate (PRR) observed as a function of modulation choice and path distance. RSS-based body area localization results are also simulated and analyzed in this thesis.

1.2 Motivation

This work was motivated by the need for accurate performance evaluation of communication and localization in Body Area Networks. Understanding how the body area channel propagates is very important and challenging. As we know, the IEEE 802.15.6 is focusing on wireless BANs, body area networks. However, to today, there is no widely-accepted model for wireless propagation in body area network. Various studies have been made upon this problem, but in body measurement and experiment are extremely difficult.

1.3 Contributions of the Thesis

I have contributed in two accepted conference papers, and one impending journal article. This thesis is based on the work in [22], [16] and [23].

This thesis introduces an interference controllable, repeatable real-time hardware platform consisting detailed implementation, validation and result analysis. This hardware platform using the Elektrobit PROPSim™ C8 channel emulator and the Zarlink ZL70101 Advanced Development Kit (ADK), simulating a body area network using a statistical path loss model developed by the National Institute of Standards and Technology (NIST), evaluating performance of a typical in-body sensor chipset. Link quality is evaluated by observing the packet reception rate (PRR) under three different transmission alternatives, and localization accuracy is evaluated using a 3 dimensional localization algorithm.

The relationship between packet reception rate and modulation under different path loss models and distances are observed. The modulations evaluated are binary frequency shift keying (BFSK) and two quadrature frequency shift keying (QFSK) differing in raw data rate. Packet reception rate shows BFSK rate has better performance and can attain good performance in longer distance. This provides a metric for how to choose modulation when performing applications for body area networks.

RSS-based localization is performed with multiple base stations on the surface of human body and one deep tissue implant. By dividing localization area into three-dimensional rings, the intersection of multiple rings provides the estimated location of the implant. By comparing the observed localization error with Cramér-Rao Lower Bound, we find that the algorithm yields accurate localization performance.

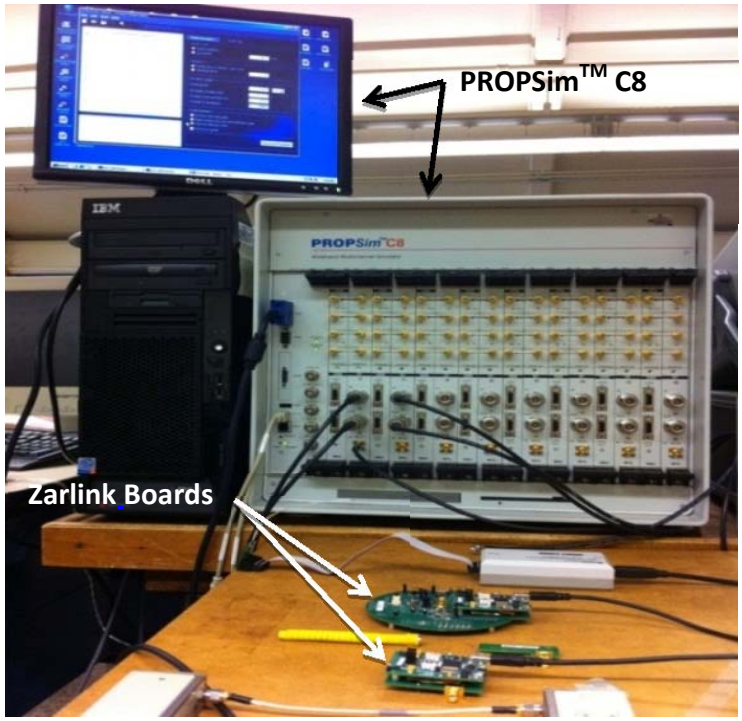

Figure 1 Major Components of Hardware Platform. The eight channel wirdeband multipath simulator with an monitor is Elektrobit PROPSim C8; Two boards are Zarlink base station and implant boards.

1.4 Thesis Outline

This remainder thesis is organized as follows. Chapter 2 defines Body Area Networks and provides background information on BANs communication and localization. Chapter 3 provides a detailed introduction of our hardware platform and our study undertaken to prove its validity. Chapter 4 presents link quality and comparisons for different scenarios to evaluate the communication performance of Body Area Networks. Chapter 5 discusses localization scenario, geolocation algorithm, and evaluates localization error as a function of in-body sensor location. Chapter 6 summarizes our conclusions. Appendices A and B demonstrated technical information on the PROPSim and Zarlink tools, respectively.

Chapter 2: Wireless Access for BAN Applications

In this chapter, we discuss wireless access for BAN applications. Section 2.1 provides a brief overview of Body Area Networks. Section 2.2 presents the channel model characteristics and IEEE task group models for BAN. Section 2.3 describes earlier work related to this thesis, work performed in WPI's CWINS laboratory and in other organizations as well.

2.1 Characteristics of BANs

The development of wireless BAN technology started around 1995, when wireless personal area network (WPAN) technologies were being considered for communications on, near and around the human body. Later, around 2001, this application of WPAN came to be identified as Body Area Network to emphasize the focus on communications on, in and near the body only.

Body area network is expected to be the next breakthrough invention with great potential due to the rapid growth in physiological sensors, low power integrated circuits and wireless communication. A number of intelligent physiological sensors can be integrated into a wearable wireless body area network under computer assistance to serve for rehabilitation or early detection of medical conditions. Unlike indoor and outdoor wireless communication, these are many challenges for body area networks [24], such as:

- ◊ *Interoperability:* implementing a plug and play device with easy interaction.
- ◊ *System devices:* designing medical device and system.
- ◊ *System and device-level security:* security of patient's data and resistance to tampering.

- ◊ *Invasion of privacy*: impact upon patients' "freedom" will affect the acceptance of BANs.
- ◊ *Sensor validation:* identifying possible weaknesses within the hardware and software design is very important.
- ◊ *Data consistency / Constant Monitoring*: accuracy and completeness of a patient's information is crucial for understanding a medical condition.
- ◊ *Interference:* coexistence of sensor node devices with other network devices in the same environment.
- ◊ *Cost:* implementation feasibility is a must.
- ◊ *Constrained Deployment:* minimizing impairment of patient's daily activity.
- ◊ *Consistency of Performance*: sensor measurements must be accurate and regularly calibrated.

One of the major challenges in designing sensor devices for wireless communications inside the human body is the accessibility of the transmission medium for performance evaluation. It is practically impossible to install a development module for a sensor inside the human body, and when the sensor has been designed we need expensive procedures conducted under physician supervisions in order to evaluate the performance of the sensors. In this thesis, we address these issues by introducing an interference controllable, repeatable real-time hardware platform for performance evaluation of a typical in-body sensor chipset used in most implant applications (Zarlink ZL70101 ADK operating at 402-405 MHz). This evaluation platform utilizes an existing multipath channel emulator (Elektrobit PROPSim^{TM} C8) to analyze the performance of the communication link between a sensor located inside the human body and a body mounted sensor. We show how link quality is analyzed by observing the packet reception rate under three different transmission alternatives.

Body Area Network (BAN), wireless body area network (WBAN), and body sensor network (BSN) are terms used to describe the application of wearable computing devices. In the view of IEEE802.15.6 standardization group, Body Area Networks should:

- Provide communication links in and around the body
- Allow communications between sensors, actuators and processing element
- Employ a hub allowing nodes to be simpler, have a longer life and be less costly.

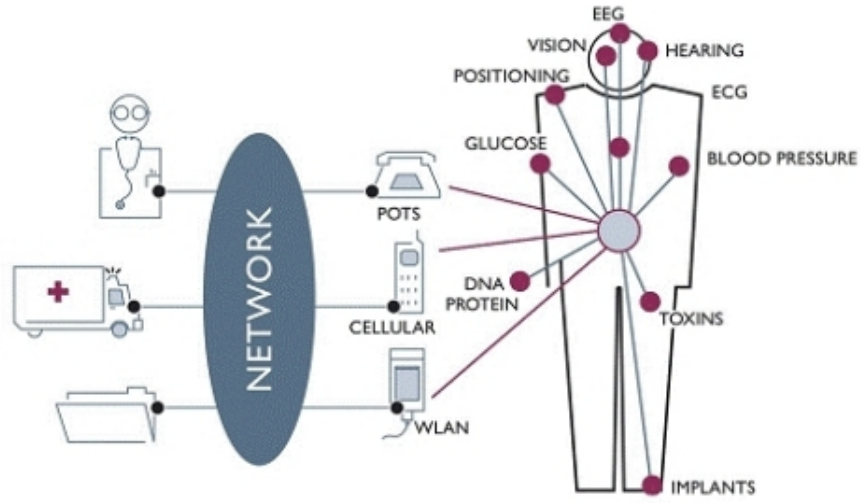

Figure 2 Body area network applications include the management of chronic disease, medical diagnostic, home monitoring, biometrics, and sports and fitness tracking.

This will enable wireless communication between several miniaturized body sensor units (BSUs) and a single body central unit (BCU) worn at the human body. The applications of Body Area Networks include many typical applications such as EEG, ECG, blood pressure and positioning shown in Figure 2, provide services regarding medical, sports and entertainment function. Here we stressed two widely concerned major applications as follows:

- A BAN network in place on a patient can alert the hospital about the impending onset of a heart attack, by measuring changes in the patient's vital signs. (Figure 3) [25]

Figure 3 IMEC demonstrated new techniques based in Eindhoven incorporate a dongle that plugs into the SD card slot of a cellphone, enabling the streaming of data from the sensors to the cellphone in real time.

- A BAN network capsule endoscopy on a diabetic patient can auto inject insulin though a pump, as soon as the patient's insulin level declines. (Figure 4) [26]

Figure 4 View the small intestine with capsule endoscopy for patients with history of obscure gastrointestinal bleeding or abnormal small intestine found on small bowel series.

2.2 Channel Model for BANs

Many efforts has been put in consider of Body Area Channel Models. [27] [28] The IEEE 802.15 Task Group 6 (BAN) is developing a communication standard optimized for low power devices and operation on, in or around the human body (but not limited to humans) to serve a variety of applications including medical, consumer electronics / personal entertainment and others. IEEE 802.15 TG6 was formed in November 2007 and began operations as TG6 in January 2008 in Taipei. It had received 34 proposals, which were merged into a single candidate proposal for the 802.15.6 Standard.

To evaluate the performance of different physical layer proposals, TG6 proposed a list of frequency band and a number of available measurements on which the model can be based, shown here in Table 1.

Table 1 List of Frequency Band

DESCRIPTION	FREQUENCY BAND
Implant	402-405
On-Body	13.5 MHz
On-Body	5-50 MHz (HBC)
On-Body	400 MHz
On-Body	600 MHz
On-Body	900 MHz
On-Body	2.4 GHz
On-Body	3.1-10.6 GHz

TG6 defined three types of BAN nodes for detailed study:

1) *Implant node:* A node that is placed inside the human body. This could be positioned immediately below the skin or deeper inside the body tissue

2) *Body Surface node*: A node that is placed on the surface of the human skin or at most 2 centimeters away from the surface
3) *External node:* A node that is not in contact with human skin (positioned from a few centimeters up to 5 meters away from the body)

Based on the frequency band listed on Table 1 and location of the communicating nodes, IEEE 802.15.6 has summarized seven scenarios for Wireless Body Area Networks propagation model. Different frequency band and channel models are evaluated widely. [29] [30] [31] In this thesis, we focus on the channel model for Medical Implant Communication Service (MICS) band (402-405 MHz), which is CM1 and CM2. MICS band has a frequency band between 401 and 406 MHz in communication with medical implants. Applications using such bandwidth are a pacemaker or other electronic implants. In order to reduce the risk of interfering with other users of the same band, the maximum transmit power is as low as 25 microwatt. The maximum used bandwidth at any one time is 300 kHz, which makes it a low bit rate system compared with WiFi or Bluetooth. However, MICS gives a range of a couple of meters. [32]

Table 2 List of Scenarios and Their Descriptions

SCENARIO	DESCRIPTION	FREQUENCY BAND	CHANNEL MODEL
S1	Implant to Implant	402-405 MHz	CM1
S2	Implant to Body Surface	402-405 MHz	CM2
S3	Implant to External	402-405 MHz	CM2
S4	Body Surface to Body Surface (LOS)	13.5, 50, 400, 600, 900 MHz 2.4, 3.1-10.6 GHZ	CM3
S5	Body Surface to Body Surface (NLOS)	13.5, 50, 400, 600, 900 MHz 2.4, 3.1-10.6 GHZ	CM3
S6	Body Surface to External (LOS)	900 MHz 2.4, 3.1-10.6 GHZ	CM4
S7	Body Surface to External (NLOS)	900 MHz 2.4, 3.1-10.6 GHZ	CM4

For wireless networks, the received power can fluctuate widely due to fading effects. Here we discuss general components of wireless path loss model for channel analysis, and we describe in detail the specific channel model from National Institute of Standards and Technology (NIST) used in this thesis research.

2.2.1 Path Loss Modeling

Path loss (or path attenuation) is the reduction in power density (attenuation) of an electromagnetic wave as it propagates through space. Path loss is a major component in the analysis and design of the link budget in any telecommunication system.

Path loss normally includes propagation losses caused by the natural expansion of the radio wave front in free space (which basically takes the shape of an ever-increasing sphere); absorption losses (sometimes called penetration losses), when the signal passes through media not transparent to electromagnetic waves; diffraction losses when part of the radio wave front is obstructed by an opaque obstacle; and losses caused by other phenomena.

The signal radiated by a transmitter may also travel simultaneously along many and different paths to a receiver; this effect is called multipath. Multipath waves combine at the receiver antenna, resulting in a received signal that may vary widely, depending on the distribution of the intensity and relative propagation time of the waves and bandwidth of the transmitted signal. The total power of interfering waves in a Rayleigh fading scenario can vary quickly as a function of distance (which is known as small scale fading). Small-scale fading refers to the rapid changes in radio signal amplitude in a short period of time or propagation distance.

In the study of wireless communications, path is usually characterized by the path loss exponent, whose value is normally in the range of 2 to 4 (where 2 corresponds to propagation in

free space, 4 is for relatively lossy environments and for the case of full specular reflection from the earth's surface—the so-called flat-earth model). In some environments, such as buildings, stadiums and other indoor environments, the path loss exponent can reach values in the range of 4 to 6. On the other hand, a tunnel may act as a waveguide, resulting in a path loss exponent less than 2.

Path loss is usually expressed in dB. In its simplest form, the path loss can be calculated using the formula

$$\mathrm{L}_P = L_0 + 10\alpha \log_{10}(d) \quad (1)$$

where L_P is the path loss in decibels, L_0 is the path loss in first meter, α is the path loss exponent, d is the distance between the transmitter and the receiver, usually measured in meters, and is a constant which accounts for system losses.

Radio and antenna engineers use the following simplified formula (also known as the Friis transmission equation) for the path loss between two isotropic antennas in free space:

Path loss in dB:

$$\mathrm{L} = 20 \log_{10}(\frac{4\pi d}{\lambda}) \quad (2)$$

where L is the path loss in decibels, λ is the wavelength and d is the transmitter-receiver distance in the same units as the wavelength.

2.2.2 Effects of Multipath in Wideband Characterizing

The models discussed generally characterize the path loss of BAN devices taking into account possible shadowing due to the human body or obstacles near the human body and postures of human body. Therefore, we need to take fading effects into consideration here.

Multipath fading is caused by reflection off or loss through walls and objects in and around the transmitter and the receiver, which ultimately change the distance power gradient. Multipath fading is also called fast fading (in contrast with shadow fading, which is a consideration for long-range outdoor radio links) because the rapid instantaneous changes in the received signal power caused by fast changes in the phase of the received signal from different paths due to small movements. Thus, multipath has strong impact in the structure of channel models for BANs.

In [33], the author claims that the multipath effects are negligible in body area networks by analyzing wideband channel characteristics in the body based on the measurements and the theory of EM wave propagation and properties of dialectic materials. S21 parameters are measured between two antennas inserted in 48 different points of pig bodies. Experimental results show that severe attenuation in high frequency band and smaller time delay take place in contrast to the case of free-space propagation.

That work drew the conclusion from measurements made along the pig's body center line, that as a lossy medium, human tissue becomes a strong absorber of radio waves. The channel exhibited such a small delay spread that the multipath effect was negligible.

2.2.3 Shadow Fading

Shadow fading is the long-term average changes in the RSS caused by changes in the relative position of large objects, such as buildings in urban areas, between the transmitter and

the receiver. The actual RSS will vary around this mean value. This variation of the signal strength due to location is often referred to as shadow fading or slow fading. The reason for calling this shadow fading is that, very often, the fluctuations around the mean value are caused by the signal being blocked from the receiver by buildings (in outdoor areas), walls (inside buildings), and other objects in the environment. It is called slow fading because the variations are much slower with distance than another fading phenomenon caused by multipath. It is also found that shadow fading has less dependence on the frequency of operation than multipath fading or fast fading, as discussed later. The path loss, Eq. (1), will have to be modified to include this effect by adding a random component as follows:

$$\mathrm{L}_P = L_0 + 10\alpha \log_{10}(d) + X \tag{3}$$

Here, X is a random variable with a distribution that depends on the fading component. Several measurements and simulations indicate that this variation can be expressed as a log-normally distributed random variable. A log-normal absolute fading component ends up as a zero-mean Gaussian fading component when expressed in decibels. In Body Area Network, much empirical measurements were undertaken regarding the fading effects and characteristics. [34]

2.2.4 MICS band Path Loss Model

An accurate, verified propagation model is essential for BANs studies. Sayrafian et al. [35] at the National Institute of Standards and Technology (NIST) introduced a path loss model as shown in Equation (2) with center frequency 403.5 MHz, modeling the human body using different dielectric parameters for different organs in simulating a 3D full-wave electromagnetic field in HFSS. PL represents path loss, d is the distance between the transmitter and receiver, S is

shadow fading which subjects to Gaussian distribution here. The simulation modeled four near-surface implants and two deep-tissue implants placed as transmitters inside a virtual male human body. Their general statistical path loss model is described in Table I, providing the NIST model parameters for different channel conditions.

For BANs, nodes situated away from the human body should also include free space path loss and additional loss caused by apparel. In the NIST work, in-body to in-body and in-body to out-of-body propagation effects were treated separately. Their work was adopted by the IEEE 802.15 task group TG6 on BANs. Therefore, we have applied four NIST channel models in this thesis.

$$PL(d) = PL(d_0) + 10nlog_{10}\left(\frac{d}{d_0}\right) + S \tag{4}$$

$$S \sim N(0, \sigma_s), \;\; d_0 = 50mm \tag{5}$$

In equation 5, PL represents path loss, d is the distance between the transmitter and receiver, S is shadow fading which subjects to Gaussian distribution here. Their general statistical path loss model is described in Table I, providing the NIST model parameters for different channel conditions. Figure 5 is the scenario from NIST to generate path loss model using Ansoft HFSS software.

Table 3 NIST Path Loss Models

IMPLANT TO BODY SURFACE	PATH LOSS (dB)	n	σs (dB)
Deep Tissue	47.14	4.26	7.85
Near Surface	49.81	4.22	6.81
IMPLANT TO IMPLANT	PATH LOSS (dB)	n	σs (dB)
Deep Tissue	35.04	6.26	8.18
Near Surface	40.94	4.99	9.05

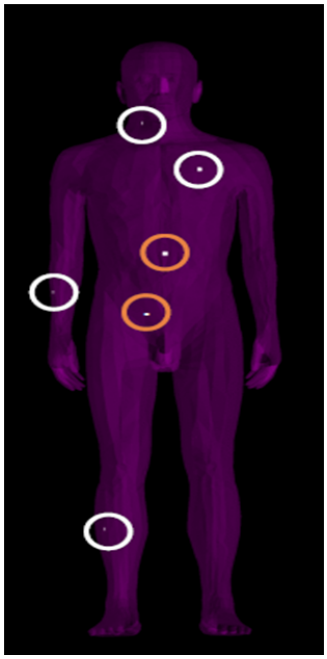

Figure 5 NIST Path Loss Model Simulated Scenario.

Near Surface Implants defined by NIST are: ICD and Pacemaker (Left Pectoral Muscle), Vagus Nerve Stimulation (Right Neck & Shoulder), Motion Sensor, Right Hand, Right Leg. Deep Tissue Implants defined by NIST are: Endoscopy Capsule, Upper Stomach (95mm below body

surface), and Lower Stomach (80mm below body surface). This thesis brings into correspondence with NIST's path loss model in definition of sensors locations and types.

2.3 Previous Works

This section provides an overview of previous studies related to development of our real-time hardware platform. In our investigation into previous work we found very limited analysis of BANs using a hardware simulation/emulation platform as we have conceived it here. Therefore we have taken guidance in our present work from an earlier study carried out in WPI's CWINS Laboratory That study had been conducted under the direction of Prof. Kaveh Pahlavan.

Real-time performance evaluation of wireless local area networks (WLANs) is an extremely challenging topic. The major drawback of real-time performance analysis in actual network installations is a lack of repeatability due to uncontrollable interference and propagation complexities. These are caused by unpredictable variations in the interference scenarios and statistical behavior of the wireless propagation channel. This underscores the need for a Radio Frequency (RF) test platform that provides isolation from interfering sources while simulating a real-time wireless channel, thereby creating a realistic and controllable radio propagation test environment. Such an RF-isolated testbed is necessary to enable an empirical yet repeatable evaluation of the effects of the wireless channel on WLAN performance.

In [9] research, as already discussed in the Introduction, a testbed was developed to enable real-time laboratory performance evaluation of WLANs. This testbed utilize an RF-isolated test system, Azimuth™ Systems 801W, for isolation from external interfering sources such as cordless phones and microwave ovens, and a real-time multipath channel simulator, Elektrobit PROPSim™ C8, for wireless channel emulation. A software protocol analyzer, Wild

Packets Airopeek NX, is used to capture data packets in the testbed from which statistical data characterizing performance such as data rate and Received Signal Strength (RSS) are collected. The relationship between the wireless channel and WLAN performance, under controlled propagation and interference conditions, is analyzed using this RF-isolated multipath testbed.

Chapter 3: Design and Implementation of the Hardware Platform

In this chapter we describe a hardware platform which we developed for Real-Time Body Area Networks Performance Evaluation and in-Body Localization. While research and development in body area networks continues to attract increasing amounts of attention, it is recognized by researchers in this field that it is very difficult, if possible at all, to make RF measurements directly inside the human body. Therefore, simulation methods are seen as the best way to evaluate the real-time performance for in-body and on-body wireless networks. The most important feature of our platform is that we use hardware components, which we are able to connect to real medical devices, thus largely reproducing medical device performance as in an actual in-body application.

The remainder of this chapter comprises three main sections. Section 3.1 provides an overview of the block diagram and major elements of our hardware platform. Section 3.2 presents detailed consideration of our hardware platform design. Section 3.3 discusses our method of gathering data packets in simulation experiments.

3.1 Elements of Hardware Platform

Here we describe the major components of our hardware separately. We begin by introducing the working principle of our hardware platform.

3.1.1 Block Diagram

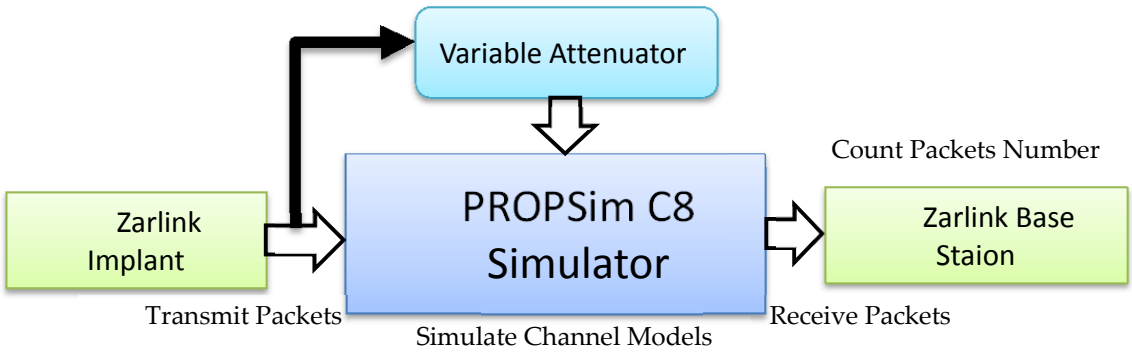

Figure 6 Functional Block Diagram of Hardware Platform for Performance.

Figure 6 is the block diagram of our hardware platform. Zarlink Implant Board (AIM100) is served as transmitter; Zarlink Base Station Board (BSM100) is served as receiver. As the channel is unidirectional, a PROPSim C8 Wideband Multipath Channel Simulator is connected between the implant board and the base station, simulating body area channel models. To simulate distance changes, the internal attenuators inside PROPSim C8 and external variable attenuators supplement this by connecting between the implant board and PROPSim simulator.

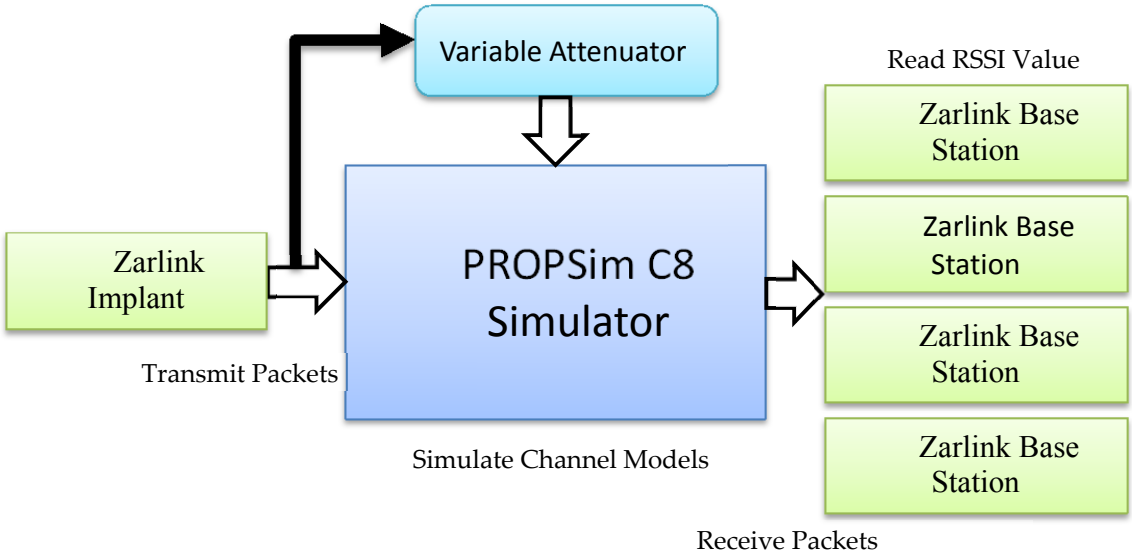

Figure 7 Functional Block Diagram of Hardware Platform for Localization.

Unlike the block diagram for communication, Figure 7 is the functional block diagram for Localization. For localization accuracy, we used 4 base stations at the same time. The AIM100 board remains serving as transmitter, transmitting medical signals constantly. Four base stations functions as receivers, recording Receive Signal Strength Indicator (RSSI) values separately. In PROPSim, among the total 8 available channels, four of them are used to simulate different channel models, each connecting to an receiver AIM100 board.

The two main components of our hardware platform for Body Area Networks consisting: the Elektrobit PROPSim™ C8 Wideband Multipath Simulator (Figure 8) and Zarlink (now a.k.a Microsemi) ZL70101 Advanced Development Kit (Figure 9).

Figure 8 PROPSim C8 Wideband Multipath Simulator.

Figure 9 Zarlink Advanced Development Kit.

3.1.1 Elektrobit PROPSim™ C8

The development of wireless systems imposes heavy requirements on product development methods and testing. Understanding the radio channel behavior is a key factor in developing wireless products that will operate properly in their intended application environments.

Elektrobit PROPSim C8 is a technology-independent radio channel emulator supporting all major wireless standards and signal types in a broad frequency range covering established and future technologies. It allows users to perform realistic and accurate radio channel emulation supporting the development of most demanding wireless applications such as beam forming, 8x8 unidirectional MIMO emulation supported with single unit, network level testing, 220 MHz-6000 MHz frequency range and 70 MHz bandwidth.

People take benefits of PROPSim's own characteristics, such as:

- Controllable multi-channel fading environment
- Repeatable lab testing facility
- Beamforming and multi-user MIMO testing capability

The PROPSim C8 plays a critical role in our platform, performing repeatable NIST channel emulation at the 403.5 MHz center frequency. It simultaneously supports simulation of eight independent RF Input and RF Output channels. Figure 3 is the front panel of PROPSim C8, from which we can observe the eight unidirectional channels and 8 RFLO (RF Local) Inputs along with LED status indicators. EB PROPSim contains a built-in PC with numbers of software for channel modeling, what are mainly used in this thesis will be described in 3.1.1.2.

3.1.1.1 PROPSim Channel Model Editor

PROPSim provides a menu of model types. If the channel model includes only one channel (i. e., one tap), then it is the so called Uni Channel Model. If the model has two or more channels (taps), the model is multi-channel model which has Direction of Arrival, Correlative and MIMO Channel as subclasses.

Because we are testing MICS bands, the center frequency is set to 403.5 MHz. In the Model Generation, we must choose maximize delay accuracy and select the “Continuous simulation” model. Mobile speed is set at a very low value, and Doppler is negligible.

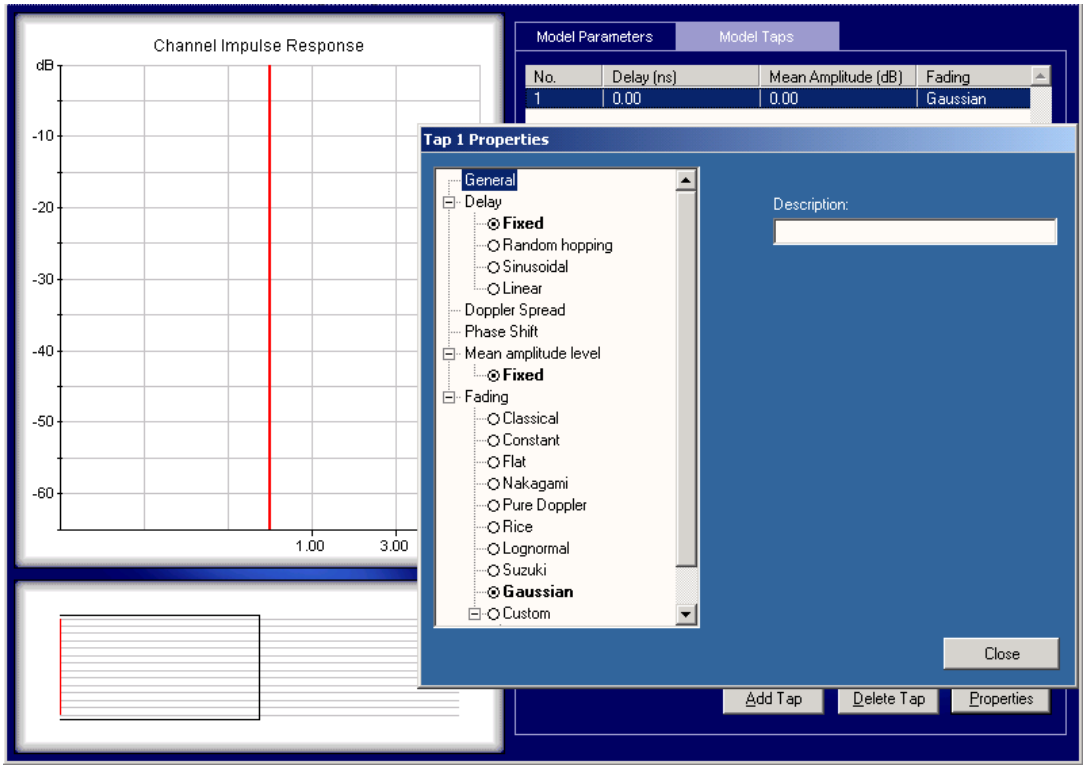

Figure 10 Configuring Model Taps Parameters.

In Figure 10, Taps means channel impulse response. If a channel model contains multiple taps, then it behaves multipath effects. For each tap in PROPSim, users are able to define delay types, mean amplitude level, fading types and parameters.

For NIST path loss model, one zero mean amplitude tap without delay is created. The fading type should be Gaussian in accordance with NIST model. After customizing, close the window and save it as "*.tap" files.

3.1.1.2 PROPSim Simulation Editor

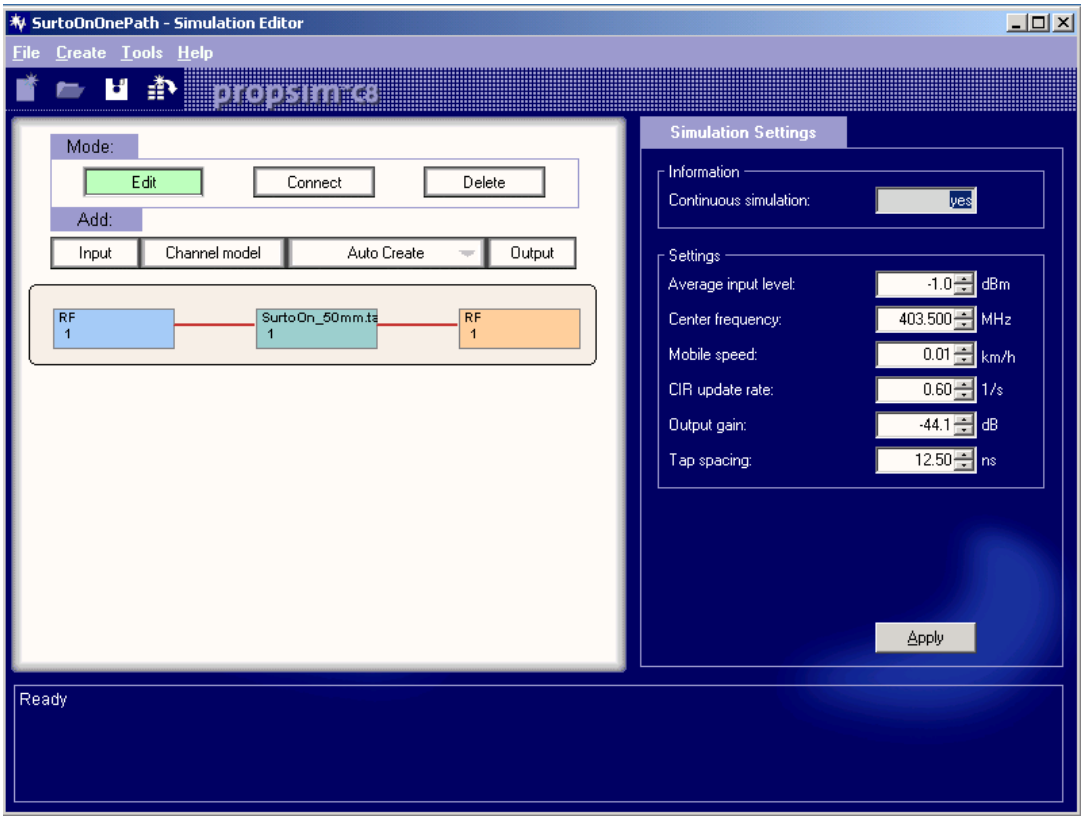

Figure 11 Simulation Editor User Graphic Interface.

Channel Model Editor is a tool help users define impulse responses, Simulation Editor is a tool help users set up channel models, define input and output and channel connection ways. Simulation Editor User Graphic Interface is given in Figure 11.

3.1.1.3 PROPSim Simulator Control

The Simulator Control Tool is used for running simulation (Figure 12). Its parameters are similar to Simulation Editor. Because one channel is used for communication, the channel number is 1. Model gain here is indicating the path loss caused channel model. If it is static channel, the model gain starts at -16 dB, since we have Gaussian fading in NIST path loss model, the model gain starts at -20.1 dB. According to equation 3 and Table 3, if we apply the deep

tissue to the body surface channel model scenario, then when the distance between transmitter and receiver is around 78 mm, we have a 49.1 dB. Add up such path loss to the Output end, the total channel gain becomes -69.2 dB which means the real power comes out of the output.

A users is able to vary attenuation at any time, being sure to select the “Apply” button whenever making a change. When finished configuring, the user selects the “Run Simulation” button at the menu bar, while being aware of any warning or errors appearing in the status window. If an abnormal state occurs, the user stops or pauses the simulation immediately and refers to the troubleshooting part of the Manual. Please see Appendix for more manipulation.

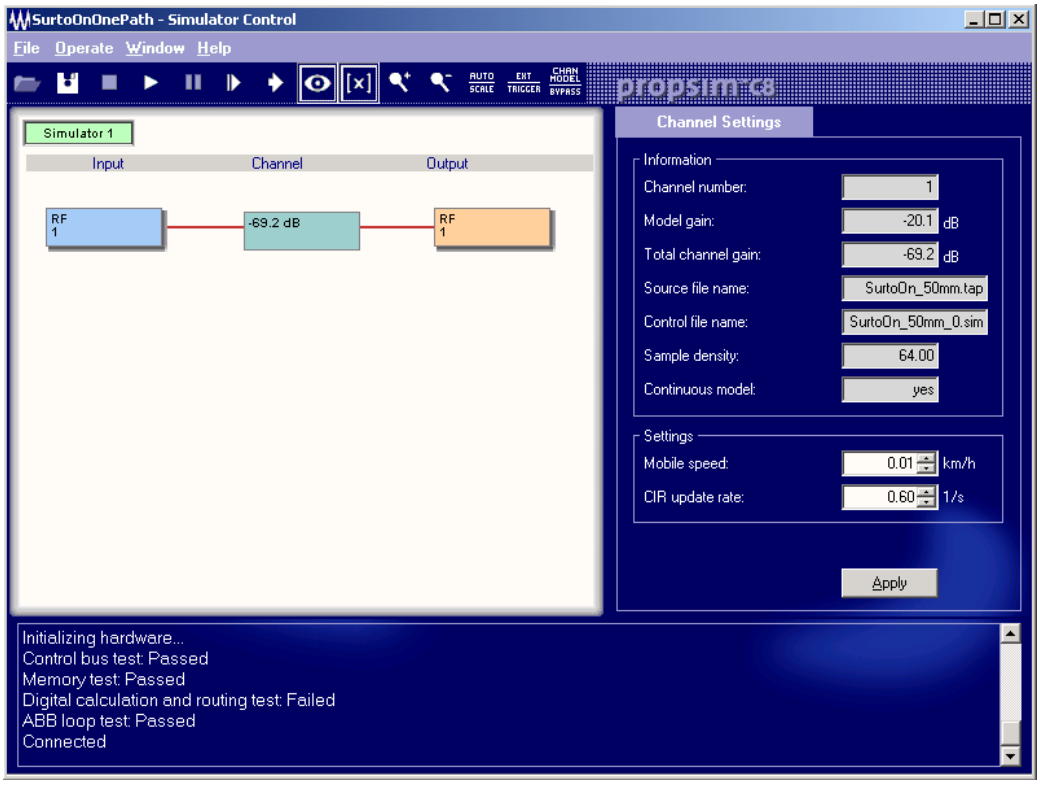

Figure 12 Simulator Control User Graphic Interface.

3.1.2 Zarlink ZL70101 Advanced Development Kit

The ZL70101 Advanced Development Kit is the medical wireless product, medical implantable RF transceivers from Zarlink Company. It is a typical high reliable, ultra-low power solution for implanted, ingested and sensor applications and external monitoring with programming equipment. The applications includes: pacemakers, implantable cardioverter defibrillators (ICDs), neurostimulators, Implantable drug pumps, bladder control devices and Implantable physiologic monitors.

The ZL70101 is very flexible and supports several low power wakeup options. Extremely low power is achievable using the 2.45 GHz ISM Band Wakeup-receiver option. The high level of integration includes a Media Access Controller, providing complete control of the device along with coding and decoding of RF messages. A standard SPI interface provides for easy access by the application.

The features and benefits of Zarlink devices are:

- 402-405 MHz (10 MICS channels) and 433-434 MHz (2 ISM channels)
- High data rate (800/400/200 kbps raw data rate)
- High performance MAC with automatic error handling and flow control, typical lower than 1.5x10.
- Very few external components (3 pcs + antenna matching)
- Extremely low power consumption (5 mA, continuous TX / RX, 1 mA low power mode) Ultra low power wakeup circuit (250 nA) Standards compatible (MICS, FCC, IEC)

3.1.2.1 Applications Development Platform (ADP100) board

The Application Development Platform (ADP100) board is a bridge board with integrated USB2.0 support to allow for interfacing between a PC running the ADK GUI software and an implant or base station board. It is mounted on both Implant and Base Station boards, containing a power switch and battery.

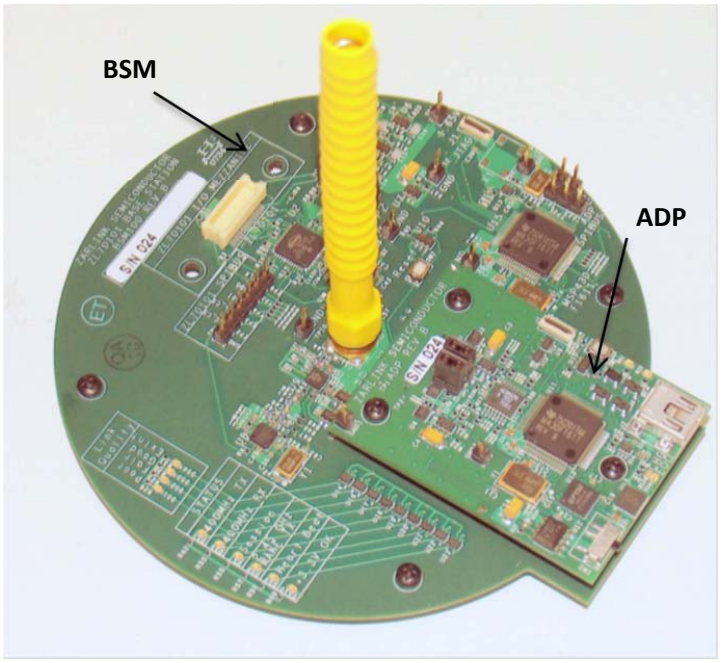

Figure 13 Base Station Module (BSM100) with Dual Band Helical Antenna. And ADP board is mounted upon BSM as power provider and controller with power switch on the lower right corner.

3.1.2.2 Base Station Mezzanine (BSM100) board

The Base Station Module (BSM100) shown in Figure 11 is composed of the Base Station Mezzanine board mated to the Application Development Platform board (ADP100). Also included is the Dual Band Helical Antenna for operation in the 2.45 GHz ISM band and the 400 MHz MICS band. On the Base Station Mezzanine, socket can connect to the MICS Test Adapter (MTA100) for viewing key ZL7010X analog and digital signals.

3.1.2.3 Applications Implant Mezzanine (AIM100) board

The Application Implant Module (AIM100) is comprised of the Application Implant Mezzanine board mated to the Application Development Platform board (ADP100). Also included is the Dual Band Printed Loop Antenna for operation in the 2.45 GHz ISM band and the 400 MHz MICS band and a MICS Test Adapter (MTA100) Mating Connector.

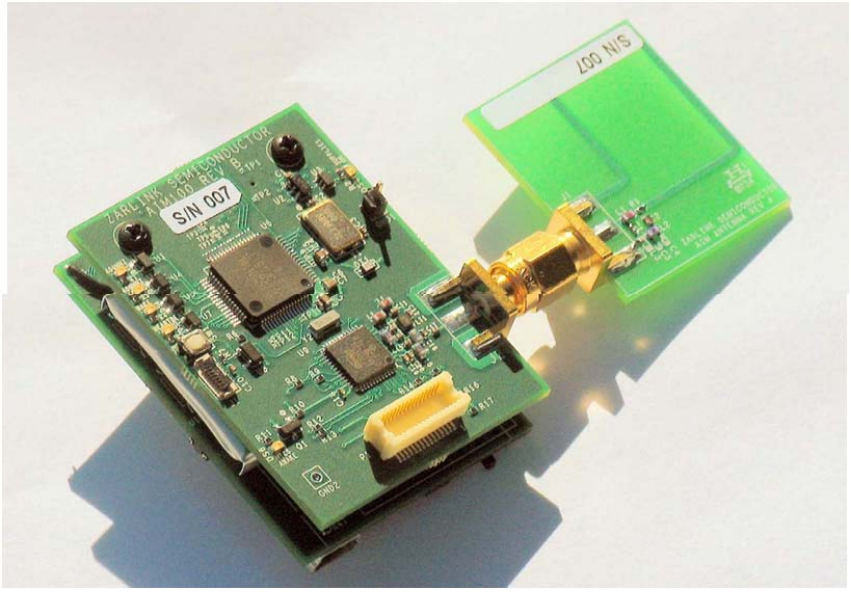

Figure 14 Base Station Module (BSM100) with Dual Band Printed Loop Antenna. An ADP board is mounted in the other side upon AIM board as power provider and controller with power switch on the lower right corner.

3.1.2.3 Programmer Cable Adapter (PCA100)

The Programmer Cable Adapter (PCA100) connects between all ZL7010X ADK boards that have the MSP430 micro-controller on-board and the Texas Instruments MSP430 USB-Debug-Interface (MSP-FET430UIF) 10 pin ribbon cable. The PLA100 allows users to download code and run the debugger to implement and test new features on the BSM100 or AIM100 boards.

Figure 15 Programmer Cable Adapter.

3.1.2.4 MSP430 USB Debug Interface

Figure 16 MSPFET430 USB Debug Interface.

The MSP-FET430UIF is a powerful flash emulation tool to quickly begin application development on the MSP430 MCU. It includes USB debugging interface used to program and debug the MSP430 in-system through the JTAG interface or the pin saving Spy Bi-Wire (2-wire JTAG) protocol. The flash memory can be erased and programmed in seconds with only a few keystrokes, and since the MSP430 flash is ultra-low power, no external power supply is required.

Note, the Zarlink board is not compatible with other USB devices, in other words, they cannot connect to the same USB network at the same time. Therefore, if we want to use this USB Debug Interface, we must unplug Zarlink boards first, and vice versa, if we want to use Zarlink boards, TI USB Debug Interface must be disconnected.

3.2 Body Area Performance Evaluation and Localization Hardware Platform Design

After giving a brief introduction and description of each component's function, this section discusses how to setup the complete hardware platform for performance evaluation and localization purpose of Body Area Network.

3.2.1 Design Consideration

These are several matters have to be taken into consideration when we design this platform.

- First, the unidirectional property of PROPSim. Because when evaluating channel performance and doing localizations, the receiver (and anchors) have no need to send information back, therefore we can use PROPSim channel directly. There is no need to add circulator in between constructing feedback path.
- Second, specification of the path loss model and how to configure channel models in PROPSim.
- Third, how to perform RSS-based localization and gather RSSI information.

We will address these considerations in details in the following section.

3.2.2 Hardware Platform Implementation

The steps of implement this hardware platform is as following:

1) Startup PROPSim C8 in advance and make sure a one and half hour warm up
2) Cabling together various components (DUTs, Zarlink Boards, PROPSim)

3) Checking the power levels at PROPSim C8 inputs, signal generator, computer connecting with Zarlink Boards.
4) Adjusting received power levels using attenuators to fit to path loss model.
5) Load path loss model with shadow fading.
6) Use a network analyzer to check the signal path and attenuation of the path, verify the output signal is desirable.
7) Switch the power on Zarlink Verifying that the Zarlink Boards was successfully connected with the computer.
8) PROPSim™ C8 (done by turning off the RF local oscillator) terminated the link
9) Increasing the path attenuation using the PROPSim output attenuators.
10) Performing measurements.

3.2.3 Assembly

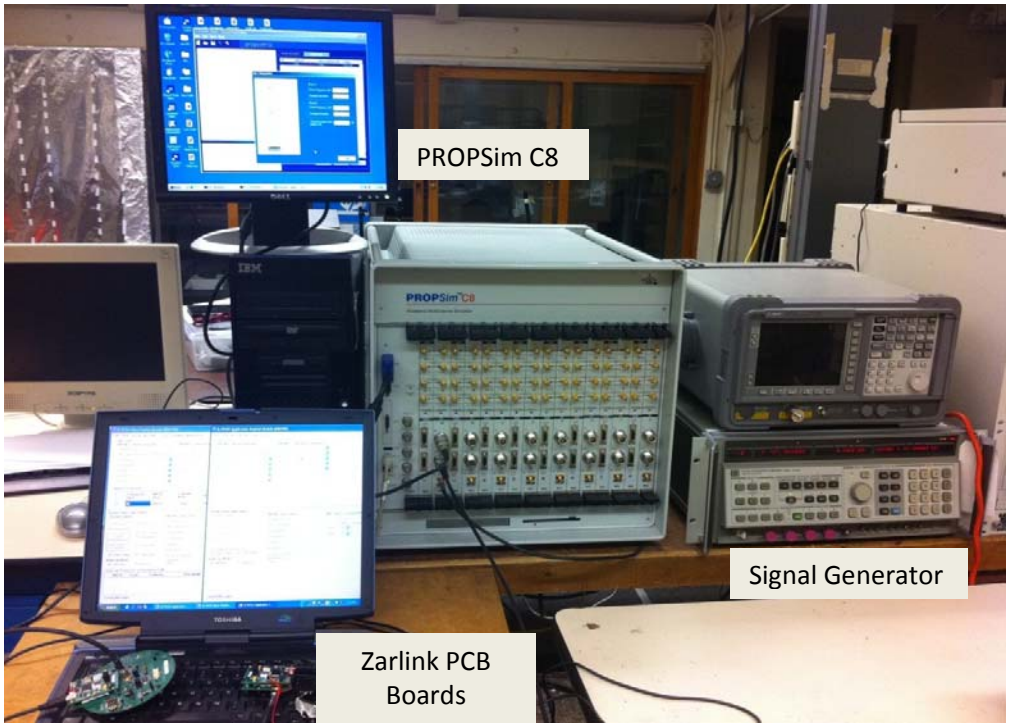

Figure 17 Assembled Hardware Platform, Zarlink boards are at the bottom left, PROPSim is in the middle.

The assembled Hardware Platform is shown in Figure 17. PROPSim C8 and a monitor connected to it are in the upper part of this figure, Zarlink Base Station Module and Application Implant Module are in the lower part of this figure. Output from signal generator is connected to RF LO port in PROPSim lower port. Zarlink Application Implant Module functions as input routing through PROPSim connected to Zarlink Base Station Module which is output. A PC laptop is used to control Zarlink boards.

3.2.4 Configuration of Channel Models

PROPSim has provided various options of channel fading, such as Nakagami, Rayleigh and Gaussian fading. In the submenu, users are able to define Doppler types including classic, round and flat. According to NIST channel models, Gaussian fading is applied in this hardware platform.

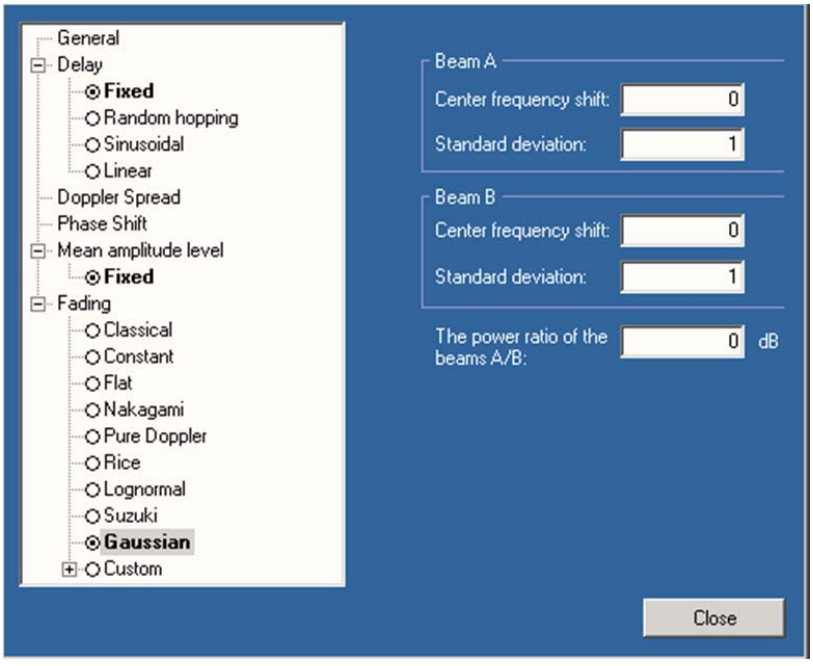

Figure 18 Gaussian fading parameter configuration.

However, in PROPSim Channel Model Editor, Gaussian fading configuration consisting 2 beams, which are called beam A and beam B shown in Figure 19. Each of them can be customized in two aspects: Beam Shift and Beam standard deviation. Another parameter which is user definable is power ratio of the beams A/B is. In this thesis, since only one normal distribution is needed, both beam shifts are set to 0. Variances of both beams are set to zero to meet the normal distribution conditions. The ratio of A/B is set to 0 dB, which is 1 in decimal unit, meaning they are equal. Accuracy verification is done to validate this Gaussian fading configuration.

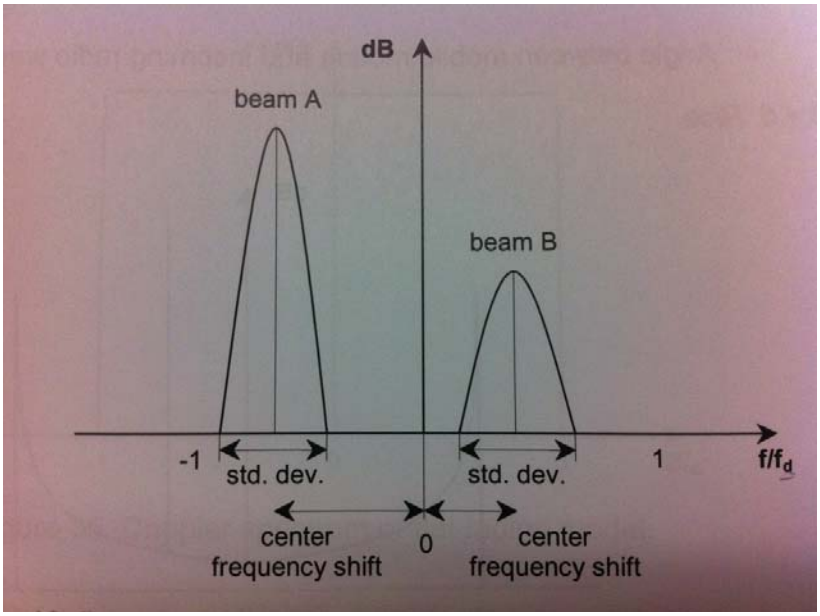

Figure 19 Doppler Spectrum of gaussian fading model in PROPSim C8.

3.3 Packets and RSSI Collection

As we know, Zarlink Application Implant Module works as transmitter, starting sending signal; Zarlink Base Station Module works as receiver, respond to received signal. In this section, we will discuss how to setup wireless access and collect data.

3.3.1 Packet Reception

To receive packet, first of all we need to let transmitter and receiver start communicate. In link performance evaluation, Zarlink Application Implant Module begin sending Emergency packets, Zarlink Base Station Module is listening for Emergency. Figure 20 is an example of emergency communication. The “Count” in “Emegency Calls” session is indicating how many packets we have received. The IMD ID is 000001 means packets are from Zarlink AIM100 with Company ID 01.

Thus, if we transmit a fixed number of packets from the transmitter at a time, the more packets we received, the better link performance is. In this example 1000 packets are sent, only 583 packets were successfully received, which is not a good result.

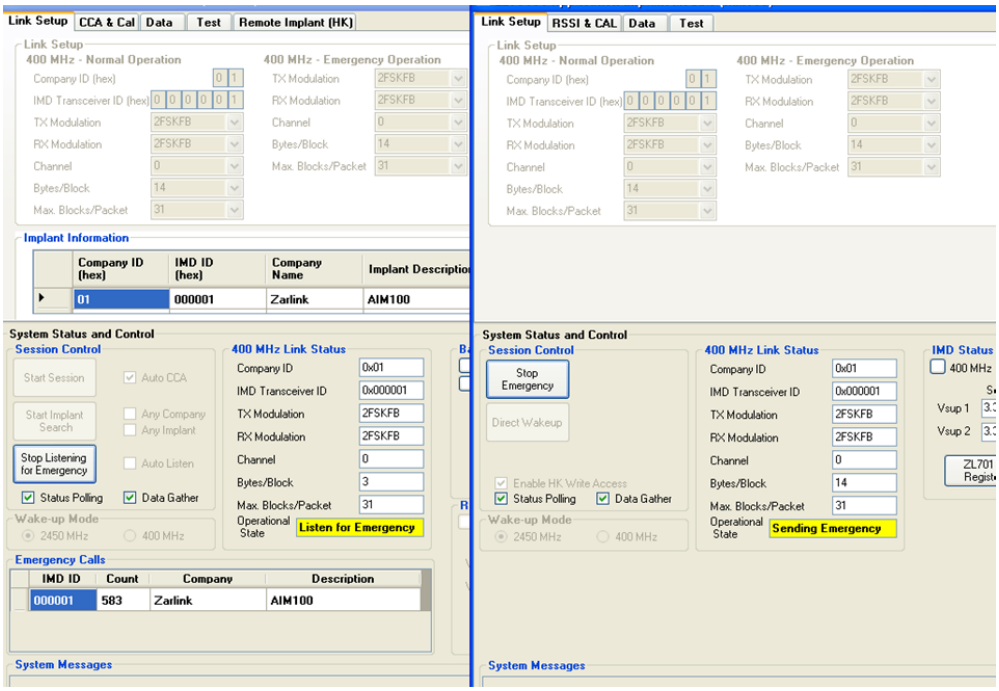

Figure 20 User Interface of Receiving Packets for Determine Packet Reception. Left is BSM100 GUI receiving and counting received packets numbers; Right is AIM100 GUI transmitting packets.

3.3.2 Receive Signal Strength Indicator

Receive signal strength indicator (RSSI) is also measured under communication status. However the method of setting up wireless access is a little bit different from section 3.3.1. In this part, as shown in Figure 21, transmitting is started by the 400 MHz carrier wave under "Test" tag by configuring which channel to be used and transmit power. Continuous RSSI measurements are performed on the receiver side. It is a decimal number varying from 0 to 31. The larger the RSSI value, the stronger the RSS strength.

Thus, if we transmitted power from four base stations corresponding to the NIST channel model's result, recorded RSSI ranging from implant at each distance respectively, an RSS database can be setup for RSS-based localization.

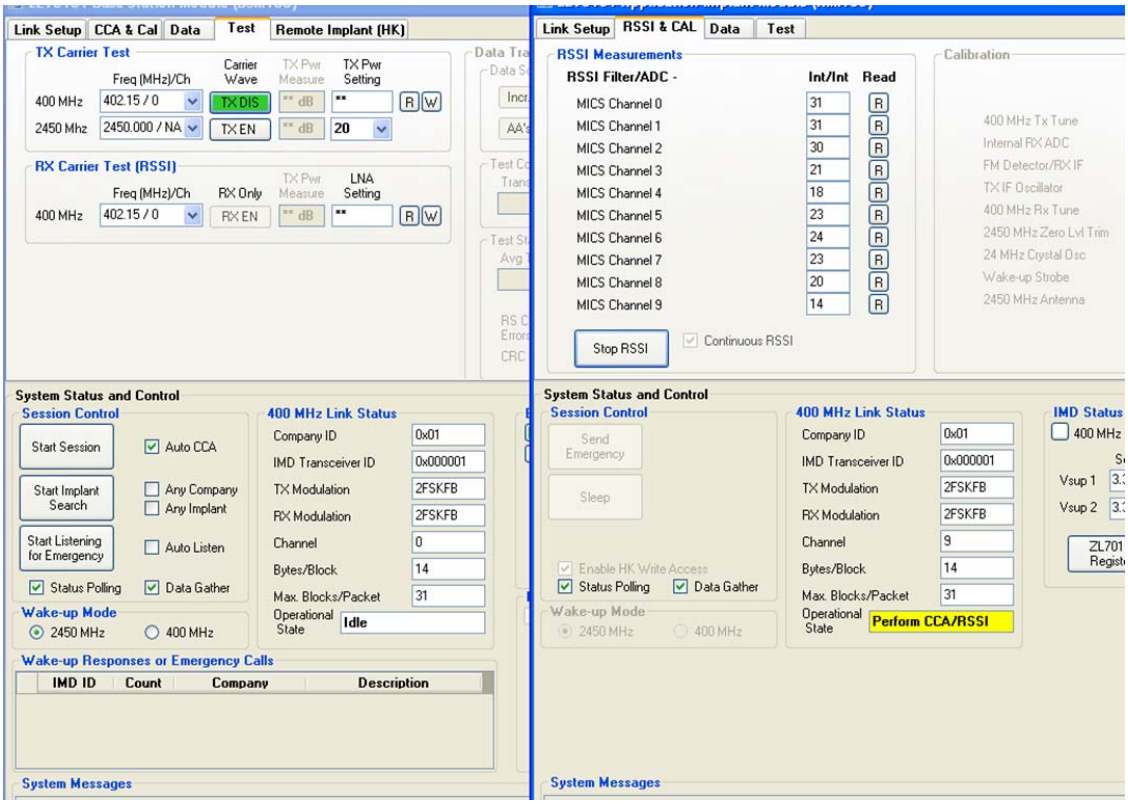

Figure 21 User Interface of Receive Signal Strength Indicator for RSS-based localization. Left is BSM100 GUI transmitting carrier wave using 400MHz channel 0; Right is AIM100 GUI reading RSSI value from channel 0.

Chapter 4: Performance Evaluation of Communication

This chapter discussed the results and analysis of performance evaluation for communication of body area networks using the hardware platform which was introduced in Chapter 3. Section 4.1 verified and validated the accuracy of our hardware platform in both perspective of path loss and fading. Section 4.2 described the scenario used in evaluating communication. Detailed results are presented in Section 4.3.

4.1 Hardware Platform Channel Model Validation

Here we verify the ability of reproducing NIST channel models utilizing our platform before producing results. The verification is very important because only if the accuracy of the platform is strictly confirmed, the results are trustworthy. The setup of the channel model consists of two parts in total: setting the power of the impulses, and choosing the fading model. Therefore, we begin by assessing the RSSI (path loss) accuracy of our platform, and then simulated fading model is compared with NIST channel model.

4.1.1 Path Loss Accuracy Verification

Here we analyze the accuracy of path loss simulating. A static channel model was under test in our platform, because we don't want fading effects influence the result. After varying path loss using platform, they are verified through spectrum analyzer and converted to RSSI according to Zarlink user manual [36]. Recording every corresponding measured discrete RSSI values from Zarlink graphic user interface, a scatter plot of RSSI can be drawn and fitted to a line. The relationships between derived receive signal strength (RSS) and RSSI line fitting from real collected data are graphed in Figure 22. Zarlink User Manual shows each step between every two continuous RSSI values differs in 2.5 dB. Since static model is used, we can observe RSSI has

small variation. Although there are still slight differences, we judge that they nearly coincide. Thus we concluded that our platform is sufficiently accurate in path loss aspect.

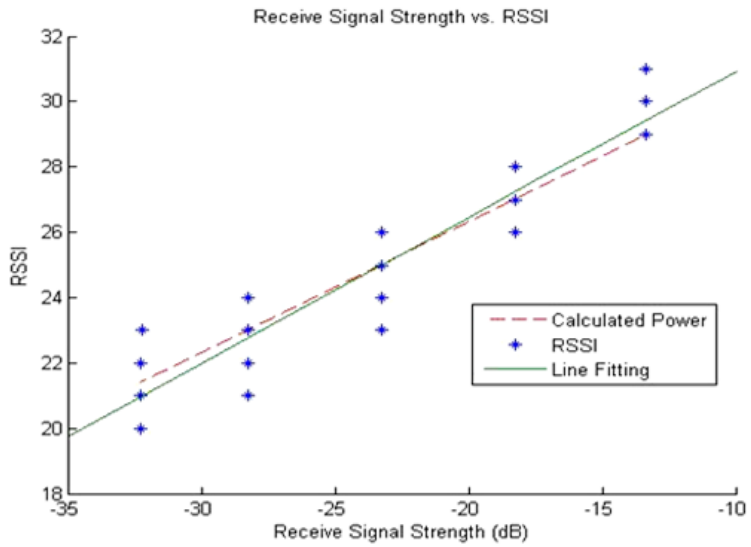

Figure 22 Relationship between RSS and RSSI. RSSI are real received power in discrete dots, RSSI line is the solid line fitting from these dots; RSS is derived from Zarlink user manual in dashed line.

4.1.2 Fading Accuracy Verification

Further verification of fading properties is done in this part. By connect Network Analyzer (Agilent Technologies E8363B) to PROPSim as transmitter and receiver, respectively, simulated channel propagation through platform is observed. Gaussian fading defined in

Table 3 was added in our hardware platform using PROPSim C8. Due to fading effects, path loss varies dramatically at any fixed range. The implant to on-body surface channel model is presented as an example. After collecting more than 500 path loss values at each TX-RX distance, a curve fitting plot of path loss was generated as shown in Figure 23 is the scatter plot from the NIST results [35].

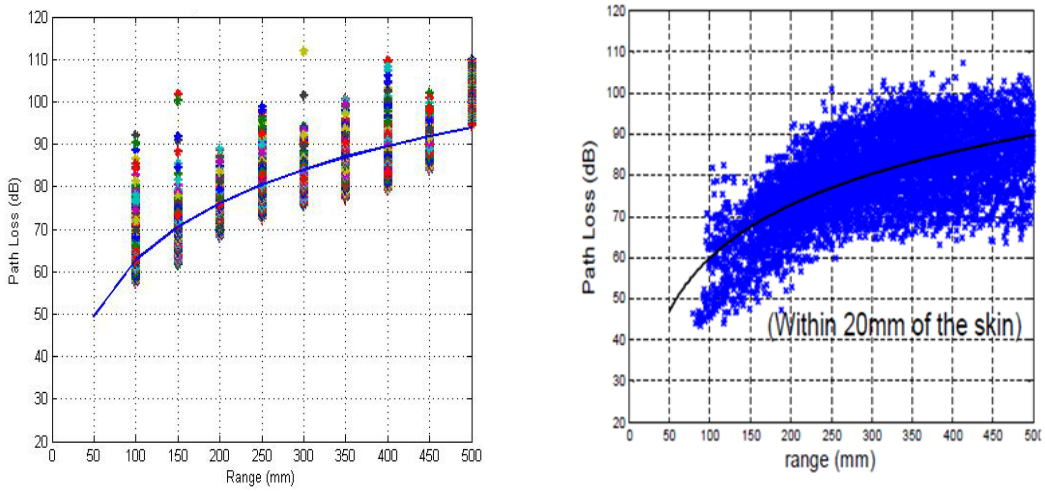

Figure 23 Comparison of Path Loss vs. Distance Scatter Plot Between Our Platform Simulation and NIST Statistical Model. Left is our result from Network Analyzer, right is NIST result used for generating statistical model.

The Probability Distribution Function (PDF) plot of RSS bias is also presented in this thesis. Figure 24 is the PDF plot of our practical measured path loss. We can observe from this figure that with normal fitting, the peak is at 0 dB representing zero-mean, standard deviation ranges from -25 dB to 25 dB, which coincide with NIST's PDF plot in [35]. Thus, our fading model is verified. Given that the path loss and fading models are both accurate, we concluded that we are able to reproduce NIST statistical channel model with our real-time hardware platform for BANs. Consequently, our platform configuration was adopted for the further results introduced in Section 4.3.

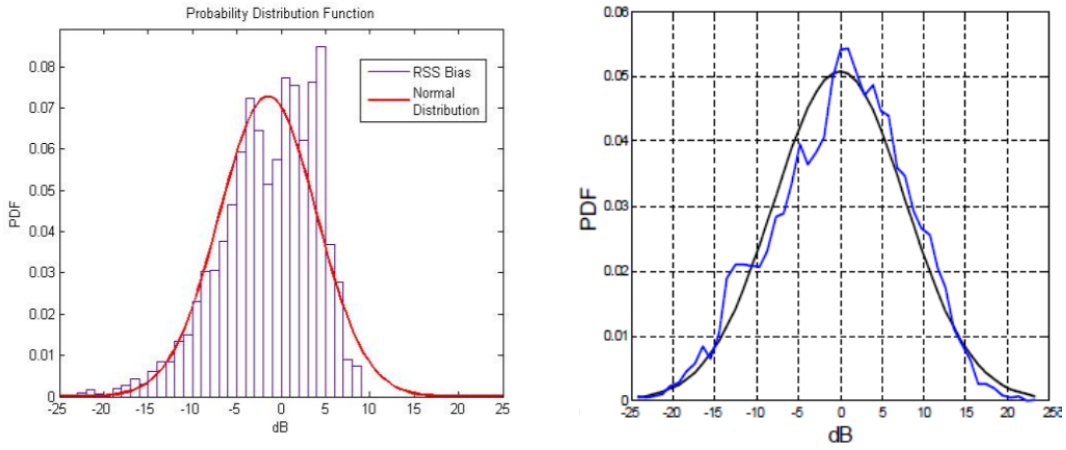

Figure 24 Comparison of Probability Distribution Function Plot Between Our Platform Measurements and NIST Statistical Model. Left is our result from Network Analyzer, right is NIST result used for generating statistical model.

4.2 Communication Performance Evaluation Scenario

Now that the platform is validated in accuracy aspect, we can prepare for starting doing measurement. Simulation scenario for communication performance evaluation is discussed in this section. As shown in Figure 25, the x-axis is aligned to the human facing direction.

Two white rings represent body implantable sensors (one is deeply implanted, while the other is implanted near the body surface) placing inside body tissue around the stomach. Two black rings represent body-wearable sensors (one on wrist, the other is above the heart) upon the body surface. Pairwise communication paths are in accordance with

Table 3.

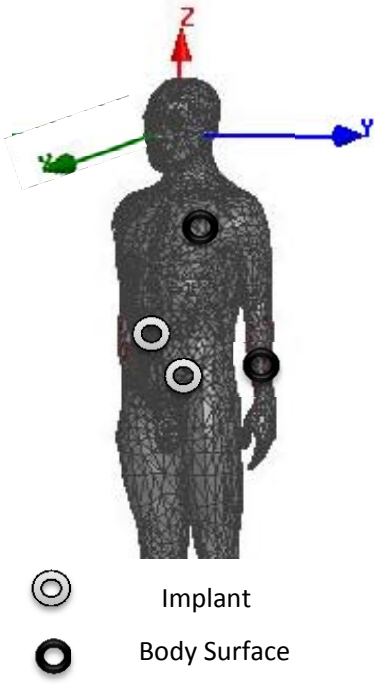

Figure 25 Simulation Scenarios of Different Sensor Nodes Locations. Include two body surface implant on arm and chest, and two deep tissue implant located lower and upper the stomach.

4.3 Performance Evaluation of BANs Communication

To establish connection, communication is initiated by the Zarlink AIM100 as indicated in Figure 24. The BSM100 works as receiver and counter, in “listening for emergency” state, watching constantly for any output packet from the Implant board. To accurately evaluate link performance, several parameters have to be fixed, such as no retransmission, -1 dB transmit power, and same packet and block length. Every emergency packet includes 31 blocks, and every block contains 3 bytes for the User PID [36].

Table 4 Modulation and Properties

CHANNEL MODULATION	RAW DATA RATE	SENSITIVITY
2FSK high sensitivity	200 kbps	-81 dBm
2FSK high rate	400 kbps	-76 dBm
4FSK	800 kbps	-70 dBm

In sight of Zarlink system configuration, three different modulations: two kinds of binary FSK (2FSK) at different data rates and 4-ary FSK (4FSK) as shown in Table 4 are discussed. Simulations were performed at 5 specific TX-RX distances: 50 mm, 100 mm, 150 mm, 200 mm and 250 mm. 20 transmissions were made at each specific TX-RX distance, 1000 packets at a time. Therefore, a total number of up to 20×1000×5×3=300,000 packets were sent for each of the four channel models.

PRR was used as benchmark in this work indicating link quality, which is an important reliability metric for communication. This ratio stands for the number of successfully received packets divided by number of total transmitted packets. The higher PRR achieved, the better the link performed.

Our results for channels through the body and inside the body are displayed separately, in view of differences between through body and in-body propagation characteristics.

4.3.1 Implant to Body Surface

Now we come to the results for communication performance evaluation, first we will discuss the Implant to Body Surface channel model category. Figure 26 shows that for any TX-RX distance tested, 2FSK high sensitivity modulation always achieves the best performance. The 2FSK high rate modulation has poorer link quality compared to 2FSK high sensitivity with lower

PRR, while 4FSK is the poorest of the three modulations. When distance is greater than 100 mm, BSM100 can hardly maintain connectivity with AIM100 using 4FSK modulation.

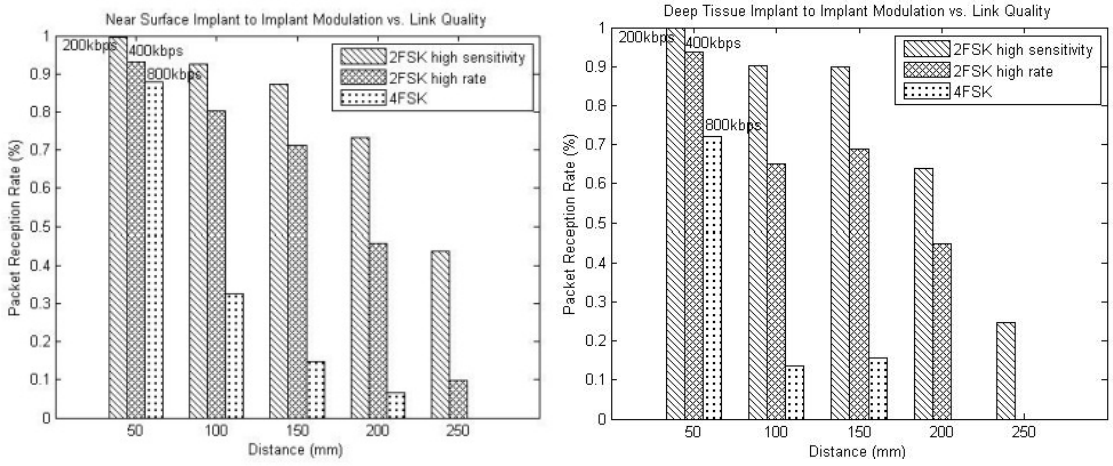

Figure 26 Implant to Body Surface Modulation vs. Link Quality. On the left is Near Surface Implant; on the right is Deep Tissue Implant.

4.3.2 Implant to Implant

In Figure 27 for Implant to Implant channel models, similar results are observed with implant to body surface in Figure 26. We can easily judge that 2FSK high sensitivity modulation always outperforms the other two. But in additional, not only the PRR of 2FSK high sensitivity is approaching 100% at 50 mm, 2FSK high rate and 4FSK also attain good performance. Moreover, even 4FSK can reach up to 200 mm, which is significantly better than seen for the implant to body surface case discussed previously. These results indicate that the implant to implant body area communication has better link quality than implant to body surface channel.

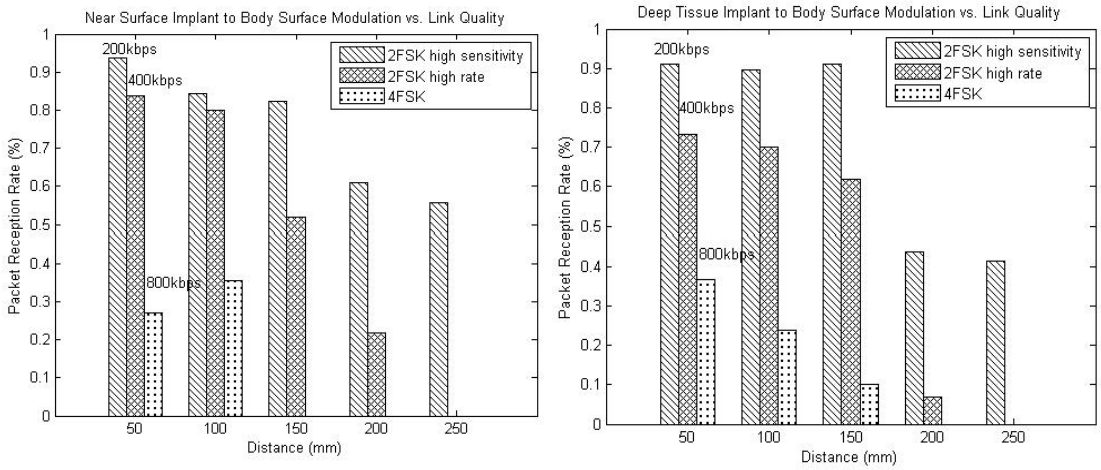

Figure 27 Implant to Implant Modulation vs. Link Quality. On the left is Near Surface Implant; on the right is Deep Tissue Implant.

4.4 Conclusion

This chapter described a real-time hardware platform for communication performance evaluation of BANs. The ability of PROPSim C8 to precisely emulate in-body wireless propagation environments has been verified in path loss and fading aspects. Zarlink boards functioned as transmitter and receiver communicating through the PROPSim C8 emulator, providing valuable insight into how BANs will perform in communications with medical implants. This emulation platform approach can be very estimable in facilitating BANs link performance assessments prior to implanting devices inside a patient's body.

Hardware platform explored the relationship between modulation selection and link performance. It shows 2FSK high sensitivity modulation has the highest PRR, i.e. better performance for the MICS band. Moreover, implant to implant channels exhibit better link quality than do implant to body surface channels. The results discussed multiple aspects which are satisfactory and desirable. Along with the repeatable, multipath and real-time properties, our hardware platform can be used extensively for various body area network scenario channel

propagation models evaluation. It also helps test and understand practical performance of medical devices implemented inside human body. With broad application foreground, our hardware platform can be utilized on other objectives, such as in-body localization, in future.

These conclusions are intuitive. Therefore our hardware platform can have good performance evaluation for in body sensor communication. It helps test and understand practical performance of medical devices implemented inside human body which software cannot. Along with the repeatable, multipath and real-time properties, it can be used extensively for various body area network scenario channel propagation models evaluation, and even body area localization as well.

Chapter 5: Performance Evaluation of Localization Technique

This chapter discussed the performance evaluation for localization of body area networks in terms of localization accuracy using the hardware platform which was introduced in Chapter 3. Section 5.1 gives a general idea of RSS-based localization. Section 5.2 describes our localization scenarios used to evaluating our localization technique. Section 5.3 presents the RSS-based localization algorithm used in this thesis. Section 5.4 discusses and analyzes the results from our hardware platform for BANs localization.

5.1 Overview of RSS-Based Localization

Receive Signal Strength (RSS)-based localization has two major algorithm. One is least square root, another is maximum likelihood. However, least square root algorithm is known to all that have poor localization performance. Thus, here we focus on the introduction of Maximum Likelihood algorithm. And the research method of bounds is discussed later.

5.1.1 Maximum Likelihood

In statistics, maximum-likelihood estimation (MLE) is a method of estimating the parameters of a statistical model. When applied to a data set and given a statistical model, maximum-likelihood estimation provides estimates for the model's parameters.

The maximum likelihood function is defined as follows:

$$L(\theta|x_1, \dots\dots, x_n) = f(x_1, x_2, \dots\dots, x_n|\theta) = \prod_{i=1}^{n} f(x_i|\theta) \quad (6)$$

where θ will be the function's variable and allowed to vary freely by considering the fixed "parameters" of observed values x_1, x_2, ..., x_n.

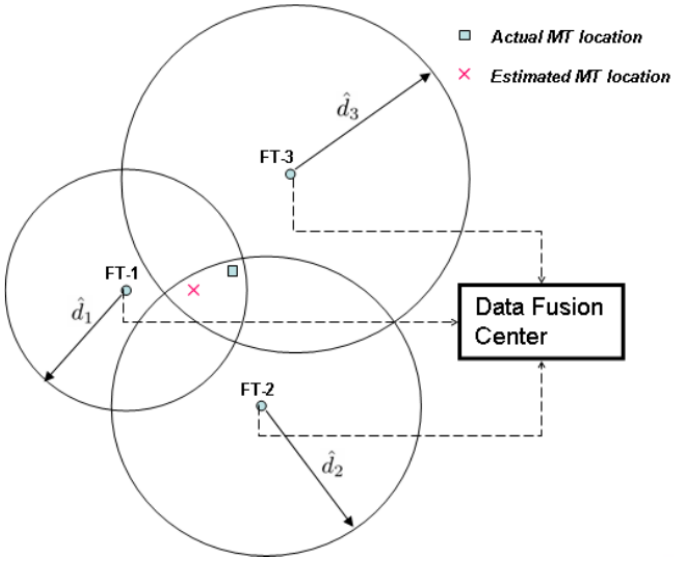

Figure 28 Illustration of a simple scenario for wireless localization.

In general, for a fixed set of data and underlying statistical model, the method of maximum likelihood selects values of the model parameters that produce a distribution that gives the observed data the greatest probability (i.e., parameters that maximize the likelihood function).

$$\{\hat{\theta}_{mlc}\} \in \{\arg max_{\theta \in \emptyset}\, \hat{l}(\theta | x_1, \ldots \ldots, x_n)\} \tag{7}$$

Maximum-likelihood estimation gives a unified approach to estimation, which is well-defined in the case of the normal distribution and many other problems. However, in some complicated problems, difficulties do occur: in such problems, maximum-likelihood estimators are unsuitable or do not exist.

Paper [37] proposes the use of a wireless sensor network for estimating the location of a transmitter that propagated over a large area. We use maximum likelihood localization algorithm (MLE) based on the concentration readings at the sensor nodes. Direct Triangulation algorithm is used to estimate the location of source. The effect of the estimation error, with different sensor number and different back ground noise, is researched by simulations. The direct triangulation algorithm is simple and intuitionistic; the MLE algorithm is robust to the much noise compared to the Direct Triangulation algorithm. The simulation results show the performance of the two algorithms that we can get accurate position of the contaminant source using the two algorithms if the sensor nodes reach to appropriate numbers in the field.

In the absence of NLOS bias (i.e., $b_i = 0$ for all i), the conditional probability density function (PDF) of $\hat{\mathrm{d}}$ in can be expressed as follows [37]:

$$\mathrm{P}(\hat{\mathrm{d}}|\mathrm{x}) = \prod_{i=1}^{N} \frac{1}{\sqrt{2\pi\sigma_i^2}} \exp\left\{-\frac{(\hat{d}_i - d_i)^2}{2\sigma_i^2}\right\} \tag{8}$$

$$= \frac{1}{\sqrt{(2\pi)^N \det(Q)}} \exp\left\{-\frac{J}{2}\right\} \tag{9}$$

where

$$\mathrm{J} = \left[\hat{d} - d(x)\right]^T Q^{-1} \left[\hat{d} - d(x)\right] \tag{10}$$

Then, the ML solution for x is the one that maximized $\mathrm{P}(\hat{d}|x)$, i.e. $\hat{x} = arg\ \max_x \mathrm{P}(\hat{d}|x)$. Note that solving for x requires a traverse over all possible maximum likelihood locations which requires intensive computationally work.

For the special case of $\sigma_i^2 = \sigma^2$ for all i, the maximum likelihood solution in $\hat{x} = arg\max_x \mathrm{P}(\hat{d}|x)$ is equivalent to minimizing J. In order to find the minimum value of J, the gradient of J with respect to x is equated to zero, yielding

$$\begin{cases} \sum_{i=1}^{N} \frac{(\hat{d}_i - d_i)(x - x_i)}{d_i} = 0 \\ \sum_{i=1}^{N} \frac{(\hat{d}_i - d_i)(y - y_i)}{d_i} = 0 \end{cases} \tag{11}$$

which are non-linear equations. Hence, x can be solved in closed form from the above two equations in Equation 11 using a least squares (LS) algorithm.

5.1.2 Cramér–Rao lower bounds

In estimation theory and statistics, the Cramér–Rao bound (CRB) or Cramér–Rao lower bound (CRLB), named in honor of the person who were among the first to derive it Harald Cramér and Calyampudi Radhakrishna Rao, [38]expresses a lower bound on the variance of estimators of a deterministic parameter. The bound is also known as the Cramér–Rao inequality or the information inequality.

In its simplest form, the bound states that the variance of any unbiased estimator is at least as high as the inverse of the Fisher information. An unbiased estimator which achieves this lower bound is said to be efficient. Such a solution achieves the lowest possible mean squared error among all unbiased methods, and is therefore the minimum variance unbiased (MVU) estimator. However, in some cases, no unbiased technique exists which achieves the bound.

The Cramér–Rao bound can also be used to bound the variance of biased estimators of given bias. In some cases, a biased approach can result in both a variance and a mean squared error that are below the unbiased Cramér–Rao lower bound; see estimator bias.

For multivariate normal distribution:

$$\mathrm{x}{\sim}N_d\left(\mu(\theta),\ \mathrm{C}(\theta)\right) \tag{12}$$

the Fisher information matrix has elements

$$I_{m,k}=\frac{\partial\mu^T}{\partial\theta_m}C^{-1}\frac{\partial\mu}{\partial\theta_k}+\frac{1}{2}tr\left(C^{-1}\frac{\partial C}{\partial\theta_m}C^{-1}\frac{\partial C}{\partial\theta_k}\right) \tag{13}$$

Where “tr” is trace.

For example, let w[n] be a sample of N independent observations with unknown mean θ and known variance σ^2

$$\mathrm{w}[n]{\sim}N_N(\theta 1,\sigma^2 I) \tag{14}$$

the Fisher information is a scalar given by

$$\mathrm{I}(\theta)=\left(\frac{\partial\mu(\theta)}{\partial\theta}\right)^T C^{-1}\left(\frac{\partial\mu(\theta)}{\partial\theta}\right)=\sum_{i=1}^{N}\frac{1}{\sigma^2}=\frac{N}{\sigma^2} \tag{15}$$

And so the Cramér–Rao bound is

$$\mathrm{var}\left(\hat{\theta}\right)\geq\frac{\sigma^2}{N} \tag{16}$$

Suppose θ is an unknown detereministic parameter which is to be estimated from measurements x, distributed according to some probability density function f(x;θ). The variance of any unbiased estimator $\hat{\theta}$ of θ is then bounded by the inverse of the Fisher information I(θ).

$$\mathrm{var}\left(\hat{\theta}\right)\geq\frac{1}{I(\theta)} \tag{17}$$

where the Fisher information I(θ) is defined by

$$\mathrm{I}(\theta) = \mathrm{E}\left[\left(\frac{\partial l(x;\theta)}{\partial \theta}\right)^2\right] = -E\left[\frac{\partial l^2(x;\theta)}{\partial \theta^2}\right] \tag{18}$$

and $\mathrm{l}(\mathrm{x};\theta) = \log \mathrm{f}(x;\theta)$ is the natural logarithm of the likelihood function and E denotes the expected value.

The efficiency of an unbiased estimator $\hat{\theta}$ measures how close this estimator's variance comes to this lower bound, estimator efficiency is defined as

$$\mathrm{e}\left(\hat{\theta}\right) = \frac{I(\theta)^{-1}}{var(\hat{\theta})} \tag{19}$$

or the minimum possible variance for an unbiased estimator divided by its actual variance. The Cramér–Rao lower bound thus gives

$$\mathrm{e}\left(\hat{\theta}\right) \leq 1 \tag{20}$$

A more general form of the bound can be obtained by considering an unbiased estimator T(X) of a function ψ(θ) of the parameter θ. Here, unbiasedness is understood as starting that $\mathrm{E}\{T(X)\} = \psi(\theta)$ in this case, the bound is given by

$$\mathrm{var}(T) \geq \frac{[\psi'(\theta)]^2}{I(\theta)} \tag{21}$$

where $\psi'(\theta)$ is the derivative of ψ(θ) (by θ), and I(θ) is the Fisher information defined above.

Apart from being a bound on estimators of functions of the parameter, this approach can be used to derive a bound on the variance of biased estimators with a given bias, as follows. Consider an estimator $\hat{\theta}$ with bias $\mathrm{b}(\theta) = E\{\hat{\theta}\} - \theta$ and let $\psi(\theta) = b(\theta) + \theta$. Therefore, any

unbiased estimator whose expectation is ψ(θ) has variance greater than or equal to $\left(\psi'(\theta)\right)^2 / I(\theta)$. Thus, any estimator $\hat{\theta}$ whose bias is given by a function b(θ) satisfies

$$\operatorname{var}\left(\hat{\theta}\right) \geq \frac{\left[1+b'(\theta)\right]^2}{I(\theta)} \tag{22}$$

From the above we can see, the unbiased version of the bound is just a special case of this result when b(θ) = 0.

It is trivial to have a small estimator that is constant has a variance of zero. But according to the above equation, the mean squared error of a biased estimator is bounded by

$$\mathrm{E}\left(\left(\hat{\theta}-\theta\right)^2\right) \geq \frac{\left[1+b'(\theta)\right]^2}{I(\theta)} + b(\theta)^2 \tag{23}$$

5.2 Empirical Indoor Localization Study

Paper [39] presents a practical RSSI based TOA ranging error model (RITEM) for localization algorithm, which can be used to estimate ranging error interval in real time. In RITEM, ranging error is classified into four classes by the RSSI value in TOA ranging process and ranging error of each class always within a certain interval. RITEM is verified by field tests in two typical indoor environments. After validation, RITEM is applied into Ranging Error Classification (REC) based TOA localization algorithm to introduce its application methodology. From experiment result, we can see that REC algorithm has improved performance in typical indoor environment in a significantly manner, comparing with LS, CN·TOAG and Nano localization algorithms.

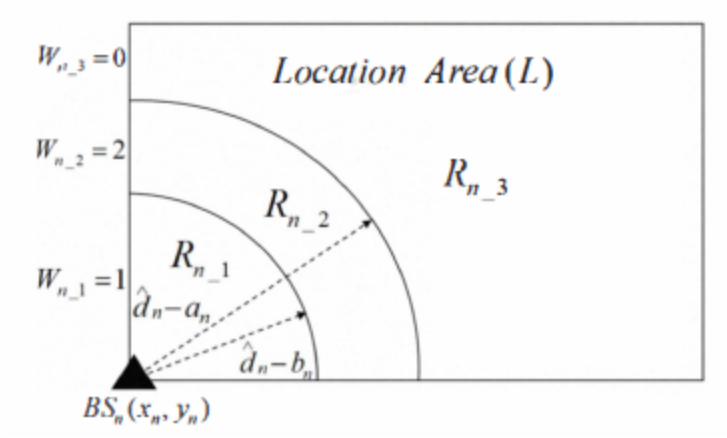

Figure 29 RITEM based location area division

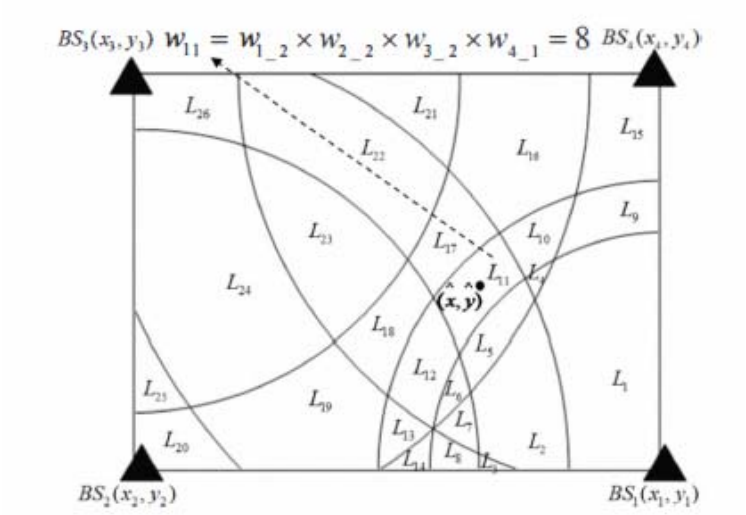

Figure 30 Maximum likelihood centroid algorithm with 4 estimated distances

The above two figures, Figure 29 and Figure 30, shows how the location area are divided according to RITEM algorithm and how the intersection occurs when applying multiple base station for distance estimating at the same time. Most probable predicted location is determined by maximum likelihood based on location area division strategy.

5.3 Body Area Localization Scenario

As the platform has already been verified previously in simulation accuracy of communication performance evaluation, here we do not need to verify again. Thus, first we will discuss the localization scenario used in this thesis. As shown in Figure 31, MATLAB is able to generate body or organ meshes by linking every individual surface point from their ".txt". The left of the figure is three-dimensional body muscle; the right of the figure is three-dimensional small intestine. The rings on the front of body surface indicate where the base stations locate. There are four base stations on the back mirroring the front ones. And red dot indicates where the implant resides.

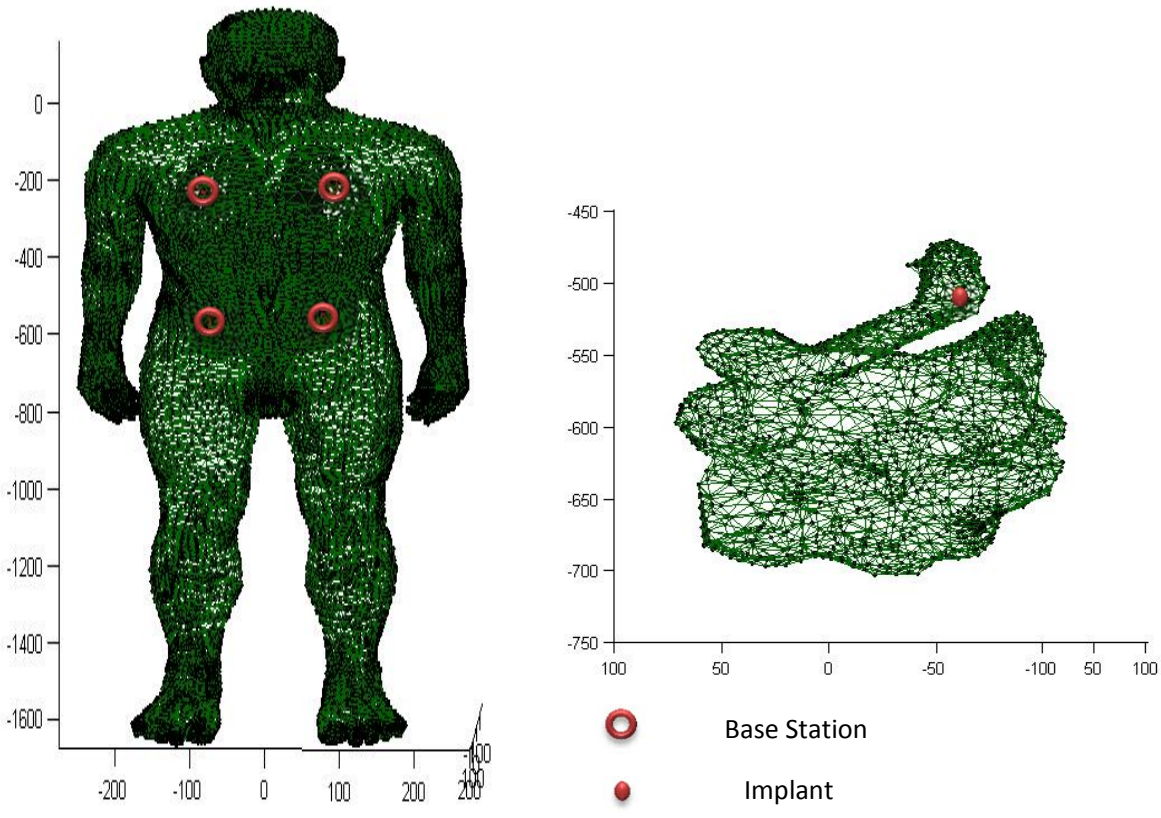

Figure 31 Simulated Body Meshes. Left is human body muscles with base station indicated by circles, right is small intestine with dot indicate where the implant is.

Figure 32 shows the overview of our scenario by putting small intestine into human body. We can observe that the small intestine is in the lower part of abdomen. The implant location is varying all along with every point of small intestine. The coordinates of these sensors are got from the MATLAB cursor function. Aiming at the place we want to attach these patch antennas, read the coordinates and record it for localization. The method for placing implant in small intestine is similar.

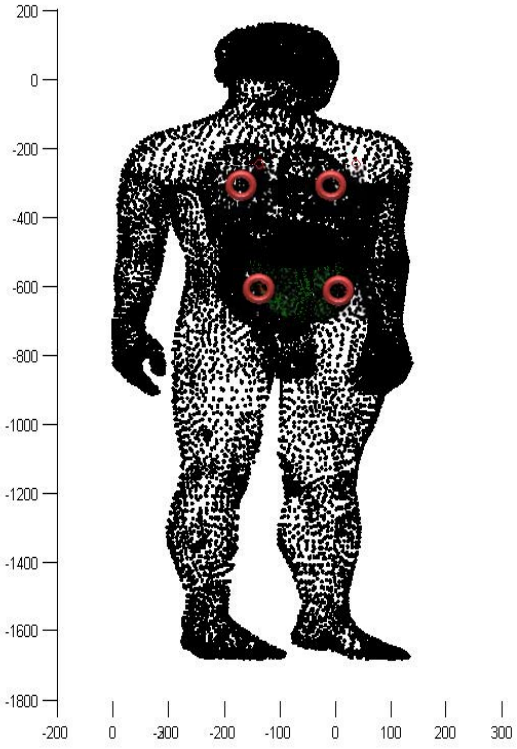

Figure 32 The human body meshes with small intestine in abdomen. The green part is where the small intestine locates; the black meshes are human body. Red circles are sensor locations.

5.4 RSS fitting for BANs

For RSS-based localization, one of the most important thing is getting the accurate receive signal strength from device under test. In this thesis, Zarlink ADK includes a function reading RSSI from Implant boards. The RSSI is defined by Zarlink Company. Here we analyze the

RSS versus RSSI on their fitting aspect. Figure 33 gives us a fitting plot and an equation derived from this fitting line. The green spots are individual RSSI values, blue solid line is fitting line. X label is RSSI without unit, y label is RSS in dB. From this Figure we can observe a clear relationship and a good fitting result. Therefore, we can use the

$$\mathrm{Y} = 1.9938 \times \mathrm{X} - 106.28 \tag{24}$$

as the converting function, where X stands for RSSI, Y stands for RSS. In other words, as long as we observe an RSSI value from Zarlink Implant board, corresponding accurate RSS value can be derived.

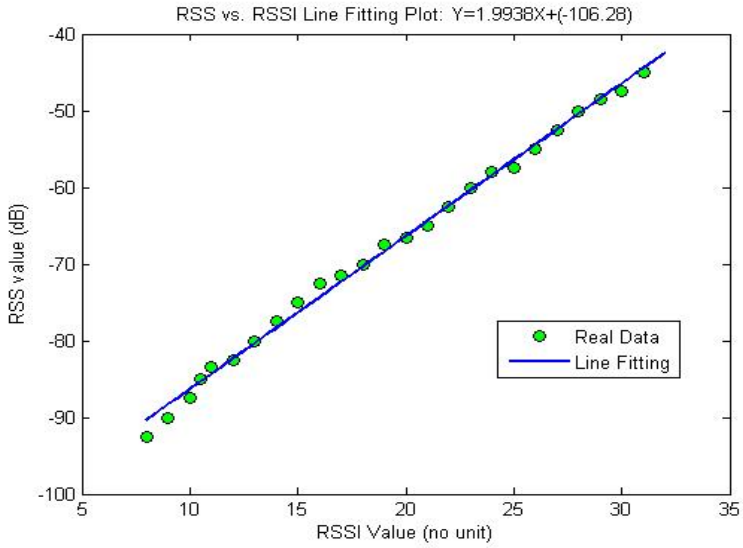

Figure 33 Relationship between Receive Signal Strength and Receive Signal Strength Indicator.

5.5 Body Area RSS-Based Localization Algorithm

In this part, an improved maximum likelihood algorithm is applied and introduced based on the localization scenario. The principle of algorithm is discussed first; its performance evaluation will be analyzed in Section 5.6.

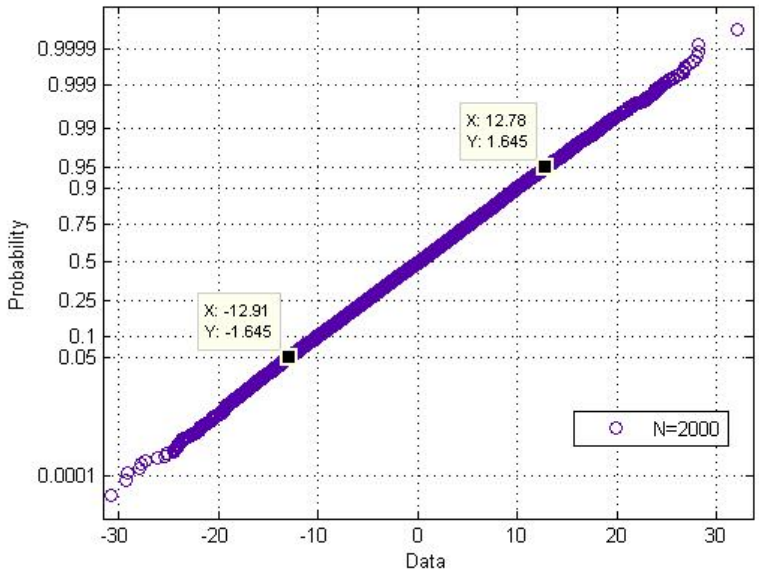

Figure 34 Cumulative Probability Plot (CDF) of random Gaussian fading added in our path loss model. X axis is the varying range of path loss in dB; Y axis is corresponding probability. In this figure, the probability is 90%.

Because in equation 4 and 5, there is always a shadow fading S influencing the accuracy of channel model, that we take a separate look at random normal distribution, which we generated 2000 sets of these rand numbers. Then we graphed the CDF plot these normal random variables. As shown in Figure 25, the x label is path loss variation rang in dB, the Y label is the probability. We limit the path loss variation from -13 dB to +13 dB here to make sure a 90% measurement successful rate, in other words, from 5% up to 95%.

By including such fluctuations in path loss model, every TX-RX distance pair will result in theoretical minimum distance D_{min} and a maximum distance $D_{max.}$ In 2D environment, the predicted D_{max} and D_{min} should looks like Figure 35.

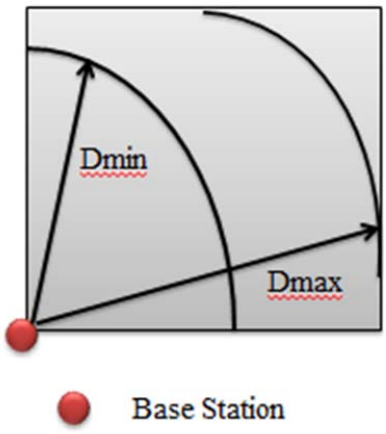

Figure 35 Maximum and minimum predicted distance in 2D environment.

Due to the fading effects, even if we only have one receive signal strength, we can have a range of possible transmitter and receiver distances. As shown in Figure 36, in three dimensional environment, the ranges looks like a ring between the maximum coverage D_{max} and minimum coverage D_{min}. Thus this algorithm divided the localization space into three parts by these sphere: R1 which is ranging inner the ring area; R2 is on and inside ring ranging; R3 is ranging outer the ring as shown in Figure 36.

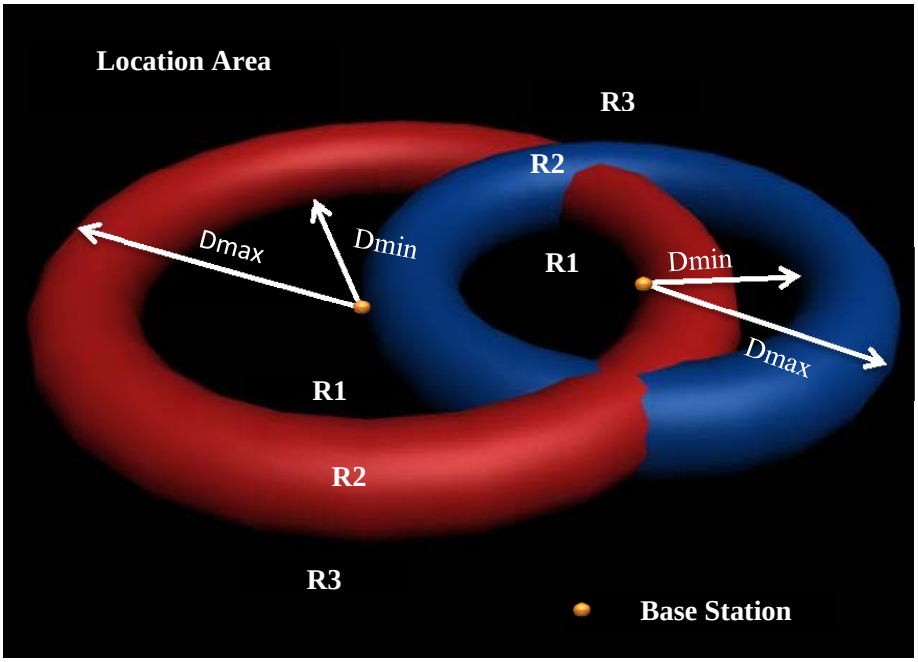

Figure 36 Maximum likelihood ranging area division. The orange dot stands for Base Station; Red and blue ring intersecting with each other are the possible ranging area of two base stations respectively.

The maximum distance D_{max} and minimum distance D_{min} are derived from the path loss model and RSSI value. If we have these two base stations merely, then the location of transmitter is predicted to be in the insect part of R2. Figure 37 give a quick glance of the predicted location. White meshes in this figure indicate the intersection of two rings. If we add another sensor as base station, very likely the third ring will only intersect with one of the white mesh. By averaging the possible location coordinates as predicted location, an extra base staion could increase the localization accuracy in a great deal. In this thesis we will use up to eight base stations for simulation to pursue a better result. Then the centroid result, i.e., the average of all intersected coordinates are predicted as the transmit source.

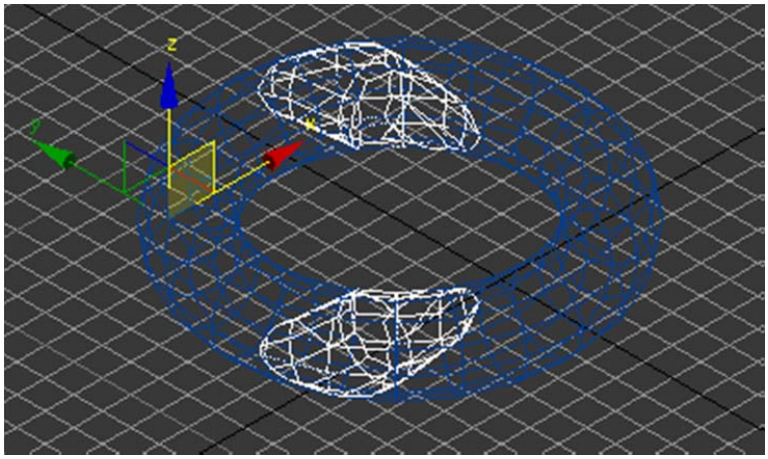

Figure 37 White mesh are the bound of where the possible source reside.

5.6 Performance Evaluation of RSS-Based localization Algorithm

In this part, we evaluate the performance and results of our localization algorithm. First we compare it with Cramér–Rao lower bound since the latter one is an important metric for valuation algorithm's accuracy and applicability.

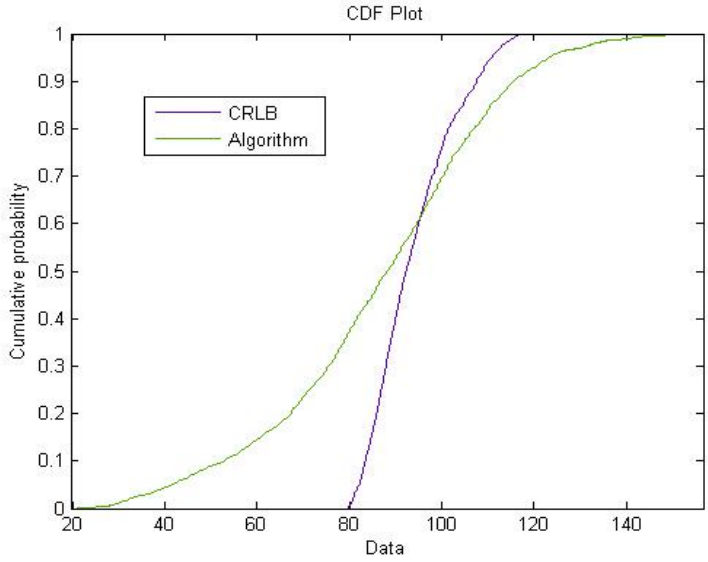

Figure 38 Comparison of CDF Plot between Cramer-Rao lower bound and Localization Algorithm with 8 base stations. The X label is localization error in mm; Y label is cumulative probability.

The above Figure 38 compared the result of 8 base stations between our localization algorithm and what of Cramer-Rao lower bound. Observation shows the result from CRLB is much more static with a small variation range from 80mm to 110mm. However the algorithm result from 30mm to 150mm. Although they are so different in ranging, their average result at 0.6 cumulative probabilities confluence.

Therefore, we explore and discuss what could be the possible reason of causing this effect. The localization errors of total 1926 coordinates are evaluated point by point firstly in Figure 39.

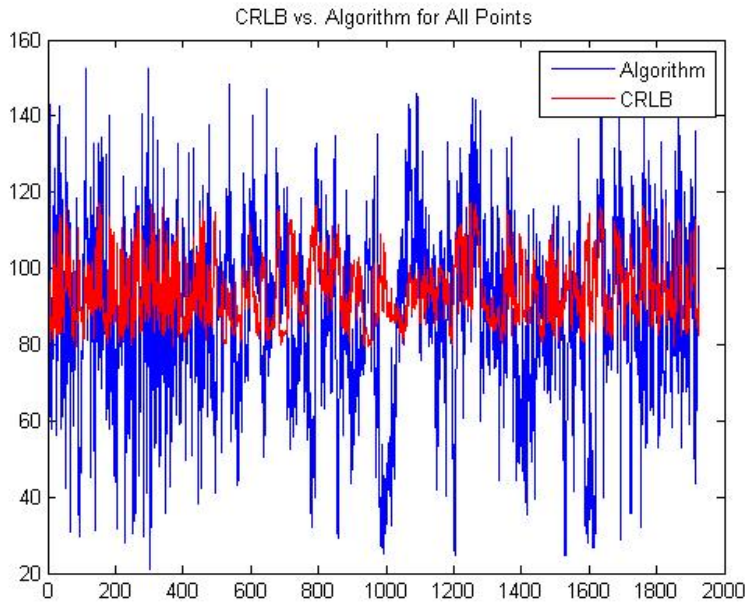

Figure 39 Point by point localization error of small intestine coordinates. X label is the point number, Y label is the localization error. Blue lines are errors of our algorithm, red is that of CRLB.

In consistent with Figure 38, CRLB result has a gentle wave while the algorithm one has severe fluctuations. To have a better understanding, we picked two points from Figure 39, one with maximum localization error whose point number is 316, the other with minimum localization error of point number 68.

Repeating algorithm several times, we can observe that on small intestine, point with minimum error always has small localization errors; point with maximum error always has large localization errors. According to Figure 39, the intersecting principle, we projected the possible locations onto the YZ-plane to look for clues of probable reasons.

Figure 40 is the minimum error point scatter plot of possible locations. Compared to Figure 44, which is maximum error point scatter plots, we can observe that Figure 40 has sparse distribution and smaller location areas which ranges about 200 mm in Y direction and 250 mm in Z direction. However in Figure 41, points distributed very closely ranging about 700 mm in Y direction and 550 mm in Y directions.

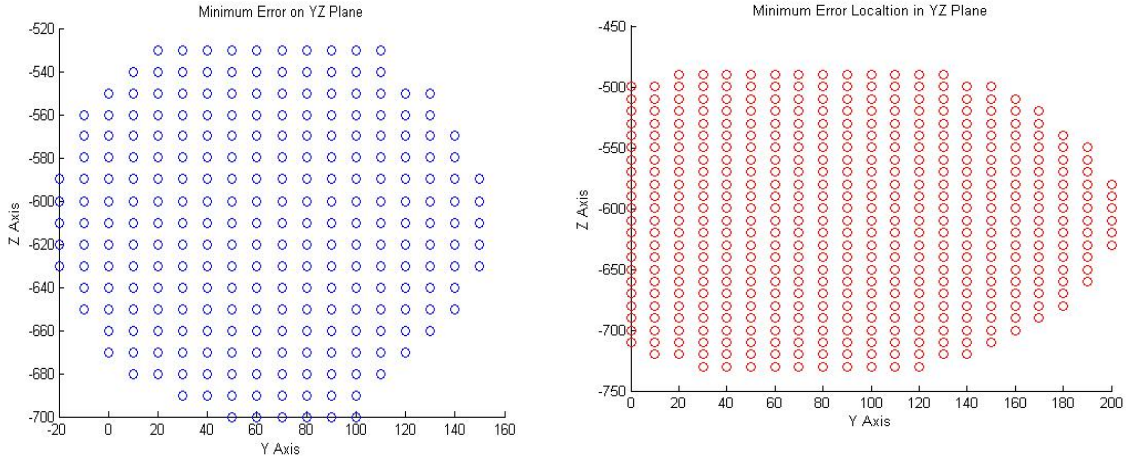

Figure 40 Minimum error point scatter plot of possible locations.

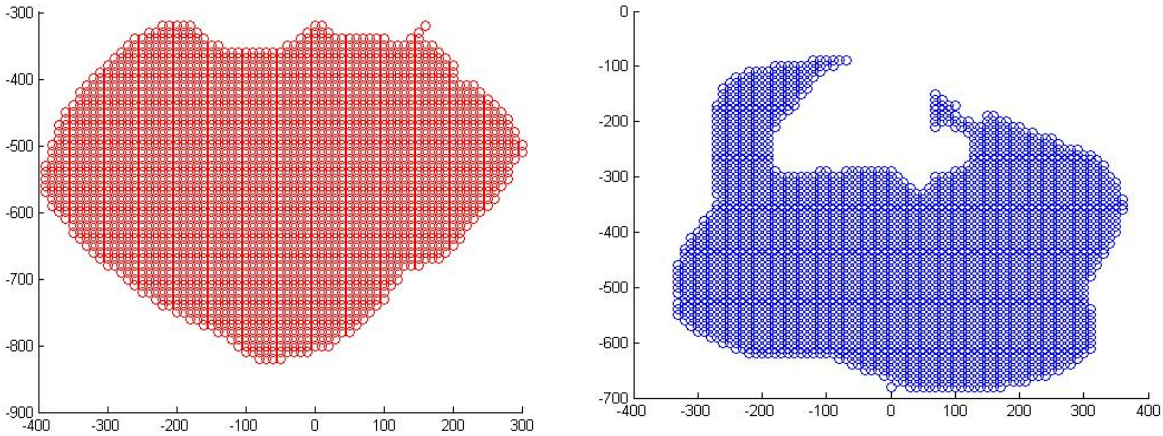

Figure 41 Maximum error point scatter plot of possible locations

We speculate that the result could be related with target locations, since the point with large errors always have bad localization performance. Therefore, the next step is to analyze these point location. Figure 42 shows the intersection of location area of Minimum error point. The red circle indicated the maximum range, green circle indicate the minimum range of each base stations. Eight base stations are in use in this figure.The right plot of Figure 42 is a closer look of the right bottom part of the left one in Figure 42. We can see there is an very small red circle limited the predicted location area.

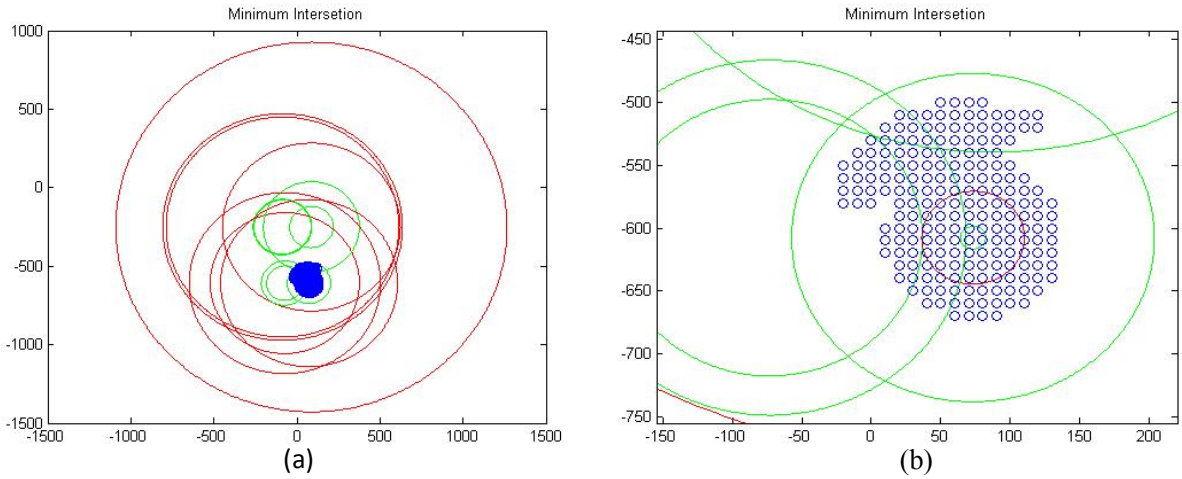

(a) (b)

Figure 42 Minimum error point intersection of location area.

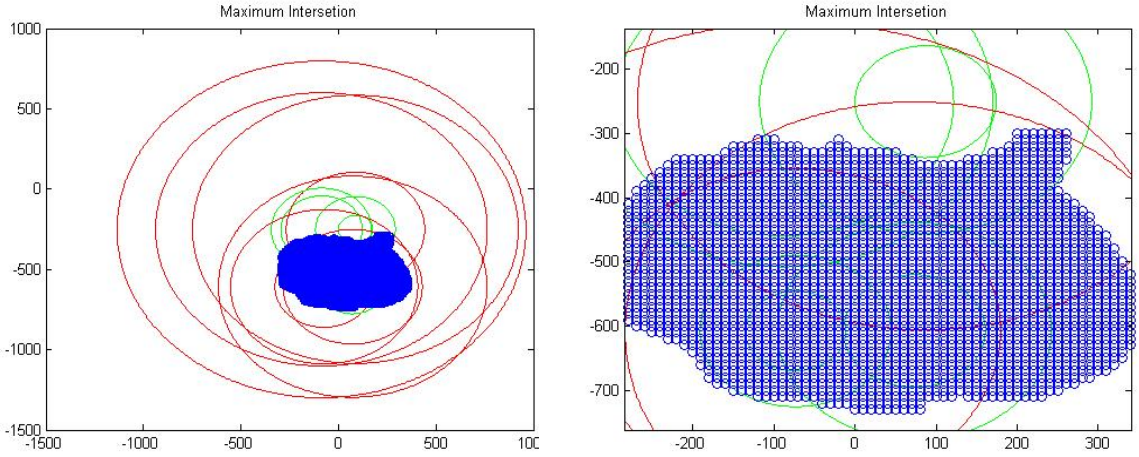

(a) (b)

Figure 43 Maximum error point intersection of location area.

The possible reason why localization scatter points looks larger than the red circle is because these maximum and minimum ranging rings are projection on to the YZ-plane. However they do have three-dimensional ranges in X direction. If we view it in 3D environment, they will intersect similar with what was described in Figure 39.

Then we take a look at the maximum error point in Figure 43. Similar to minimum error point, the left plot in Figure 43 shows all the eight ranges of different base stations, the blue part is the intersection. The right plot Figure 43 is a closer look of the left one similar to the relationship of Figure 42. We can observe from Figure 43 that the intersection part is much larger because not only the red circles, but also the green circles are larger than that in Figure 42. According to the above mentioned several reasons, we presume the minimum error point is very close to one base station, whereas maximum error point has almost equal distances.

To verify our assumption, we locate these points in human body. The left plot from Figure 44 shows the implant location when error is very small. The right plot in Figure 44 shows the implant location when error is large. Simulating it inside human body in MATLAB or combining this figure with Figure 31 and Figure 32, we can tell the position in the left of Figure 44 is very close to a base station which locates on the bottom right of human inner back, however, the position in the right of Figure 44 is in the middle of human body.

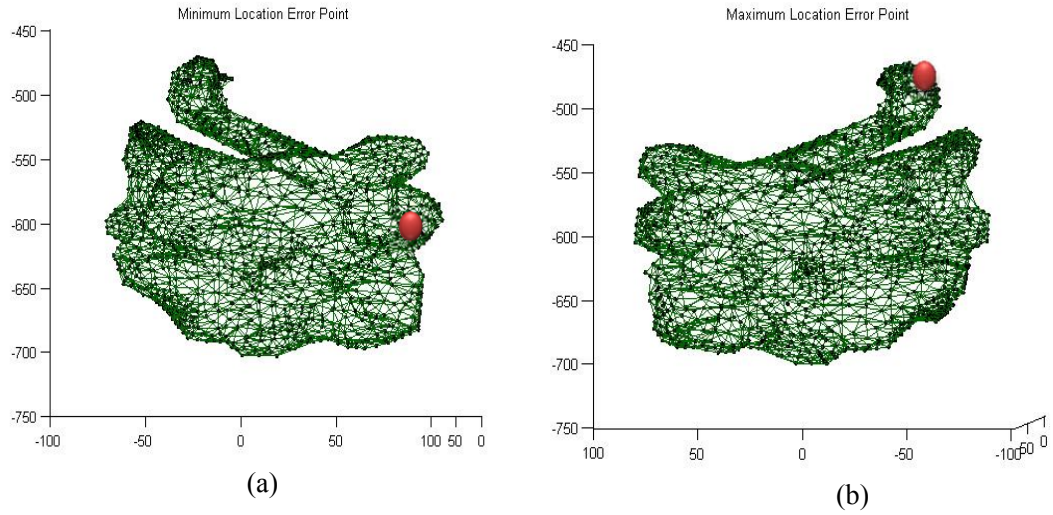

Figure 44 Maximum and minimum error point location on small intestine. The green mesh is small intestine of typical human body, red round is the implant location.

As a result, we can conclude in our algorithm, implant positions have strong impact on our algorithm performance. When the implant is close to base station, we can get even better localization performance than Cramer-Rao lower bound.

The possible reason could be that location area is limited for a small ranging. However Cramer-Rao lower bound takes whole human body into consideration to derive the bounds. It is intuitive that reducing sample areas will decrease the error.

Another reason could be that we only take part of Gaussian fading into account when calculating path loss. As shown in **Error! Reference source not found.**, apart from all Gaussian fading, only the part which has over 90% possibility is studied. This will sacrifice the probability of successful calculation, but will increase the localization performance as the shadow fading effects are restricted.

5.7 Performance Evaluation of RSS-Based Localization for Hardware Platform

This part we will evaluate the localization performance from real-time hardware platform using RSSI values read from Zarlink user graphic interface. Four base stations are used in this case.

A one set of sample RSSI values looks like the followings:

Table 5 Sample RSSI localization values from hardware platform

Base Station 1	Base Station 2	Base Station 3	Base Station 4
21	23	17	18
21	23	16	16
21	19	18	17
21	20	21	19
21	21	19	21

Every time we pick one of the RSSI values from our observation, convert them to receive signal strength, applying our algorithm to do a RSS-based localization. For the sample location, we get the standard deviation of error from our hardware platform:

44.7863 mm

which is a satisfactory performance result for in-body localization.

5.8 Conclusion

This chapter described a real-time hardware platform developed for three dimensional RSS-based localization performance evaluations of BANs. Our unique hardware platform includes multiple typical medical sensors of Zarlink base stations as receivers, and a Zarlink Implant as transmit source. First of all, we validate the received signal strength accuracy after simulation through our hardware platform. Then we introduce our improved maximum likelihood localization algorithm for the 3D ring and intersection area. The centroid data from our algorithm predicts the source position. With that, our software and hardware simulation scenarios are presented.

We compare the results from our localization algorithm with the Cramér–Rao lower bound. The result indicates our algorithm presents a satisfactory performance, however in some place the localization performance is even better than bound. Possible reasons were discussed and explained. After combining with localization algorithm, our hardware platform presents a satisfactory performance of in-body 3D RSS-based localization with multiple commercial medical sensors. Thus, our hardware platform is helpful and can be used extensively for future works.

Chapter 6: Conclusion and Future Work

In this thesis, we present a unique hardware platform for body area performance evaluation of communication and localization. Typical medical implantable devices from the Zarlink Company are tested using the channel model simulated in the Elektrobit PROPSim™ C8, which provides a real-time, interference controllable and repeatable environment. Base Station and implants serve respectively as transmitter and receiver. The thesis utilizes the path loss model from National Institute of Standards and Technology (NIST) for the Medical Implant Communication Service (MICS) band.

Our hardware platform is first validated with respect of both the path loss and fading distribution simulation ensure an accurate simulation result. Three modulations: 2FSK high data rate, 2FSK high sensitivity and 4FSK are compared in Chapter 4. Four different scenarios are categorized: deep tissue implant to body surface, near surface implant to body surface, deep tissue implant to implant, near surface implant to implant. Received packets number is counted in the receiver side to analyze packet reception rate under these different propagation scenarios and different modulations. By varying the transmitter-receiver distance under each condition, we can observe from Chapter 4 that modulation with lower data rate has higher packet reception rate, in other words, better communication performance. Moreover, implant to implant channels exhibit better link quality than implant to body surface channels. These results take multiple considerations into account which are intuitive. Therefore, our hardware platform can help provide valuable insight into how BANs will perform and how to implement devices in wireless BANs incorporating medical implants.

Analysis of body area localization is based on receive signal strength (RSS). The RSS simulation validation is conducted by fitting simulated RSS and theoretical RSS values. We can

observe our hardware platform provides accurate performing RSS simulation. Then we introduced an improved algorithm based on maximum likelihood. This algorithm was first simulated in MATLAB, along the propagation path of the small intestine. Then the observed error was analyzed and compared with the Cramér–Rao lower bound. Possible causes of the observed error performance are discussed in the thesis. Finally, a number of simulations are performed with our hardware platform, and results are analyzed by our algorithm. These results show that our hardware platform and algorithm present satisfactory performance for in-body localization. Thus, this hardware platform can be used more extensively for localization along different body organs and different sensor locations.

Due to the real-time, repeatable and controllable characteristics of our hardware platform, future work can be done on developing new body area cyber physical system. Our hardware platform is one with which one can easily interact and intuitional perceive results. This capability can be further enhanced by adding visualization components to this hardware platform.

Appendix A: PROPSim Tutorial

Here we list several notes before giving a detailed description of PROPSim software:

(1) Make sure the monitor and mouse is correctly connected. Otherwise we will lose control of the PROPSim and have to force shut down, which is harmful for the machine.

(2) Do not connect the simulator to an AC power source before verifying that the line voltage is correct.

(3) Allow the simulator warm up to room temperature before turning the power on. Turning on a cold simulator may damage it because of possible water condensation.

(4) Ensure at least one and a half hour warm-up before running simulation which demanding high accuracy.

(5) Ensure the simulator has unrestricted airflow for the fan and ventilation openings in the rear cover and bottom panels since the inner PC is dissipating heat.

(6) Always beware of the RF IN and IN RFLO signal. If it is too high, over 0 dB, simulator will be damaged.

(7) Constantly check the Status LEDs all the time during the experiment. The number 10 LED is POWER, indication system status. If it is RED, there is ERROR. We will need to shut down and restart system. The number 18 LED is STATUS. If it is RED, it means the input signal is too high. We must stop simulating and disconnect circuits as soon as possible. The number 19 LED is also called STATUS, it shows RFU (Radio Frequency Units) status. This kind of LED on the top of

eight RF IN port works alike LED 18. If the input signal is too high, it becomes RED, we must prevent this happening. If it happens, disconnect and stop simulating immediately.

After checking over the above seven rules, we can now start using PROPSim in a safe condition.

In this thesis, because NIST path loss model need only one channel, we select “Uni Channel Model”. Then click “Next”.

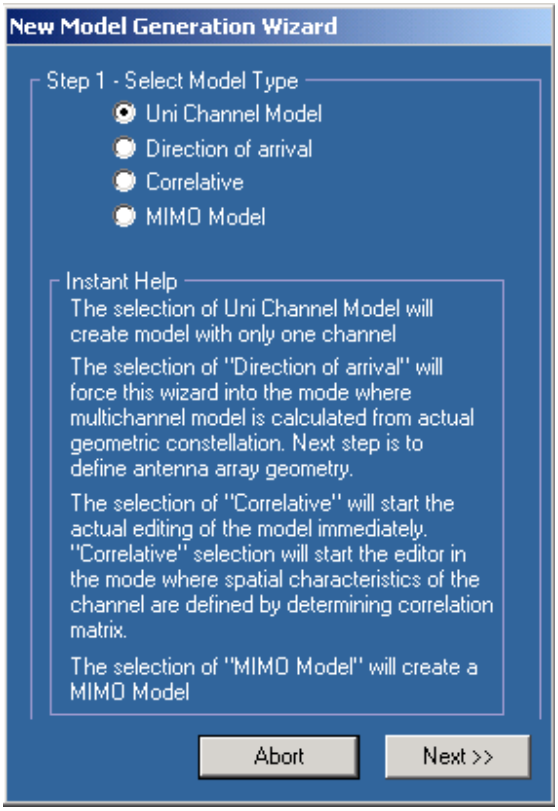

Figure 45 Channel Model Types Selection.

Users are able to customize center frequency, channel power delay profile parameters, including mean amplitude level, delay and phases of multipath components, fading types and other parameters in Chanel Model Editor.

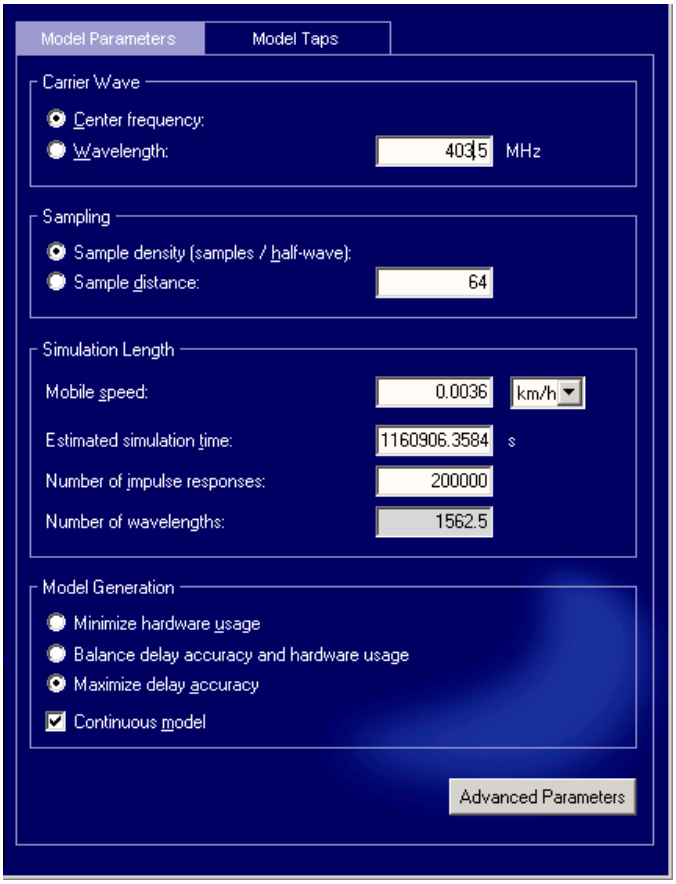

Figure 46 Configuring Channel Model.

In accordance with channel model editor described previously in Chapter 3.1.1, the center frequency is 403.5 MHz. Average input level is set to -1 dBm. The "*.tap" file we just generated in Channel Model Editor is loaded into Simulation Editor as channel model, connecting with input and output. When the Simulation Editor has finished configuration, a "*.smu" file along with "*.sim" and "*.ir" files should be generated. These files are used for performing simulation.

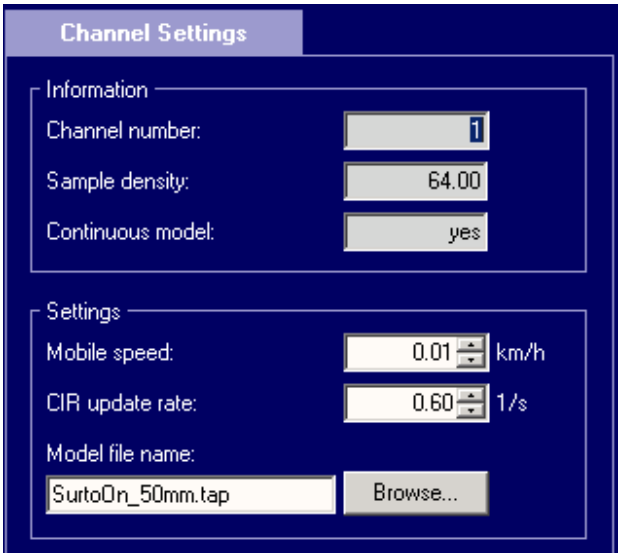

Figure 47 Channel Settings for Generate Simulation

Appendix B: Zarlink Tutorial

This section describes in detail the operation of the main components of the ZL70101 ADK – the BSM100 and the AIM100. These features are important in Zarlink operation.

The ZL7010X Application Development Kit main form controls the launch of the ADK application and its components. It provides revision of the software and also controls system level timing intervals for various functions described below. The BSM100 and AIM100 button are used to launch their own interface. System setting control the interval of timers used for various operations of the system. The range of these settings is from 0.5 Hz to 10 Hz.

B.1 Base Station Module (BSM100) Main Form

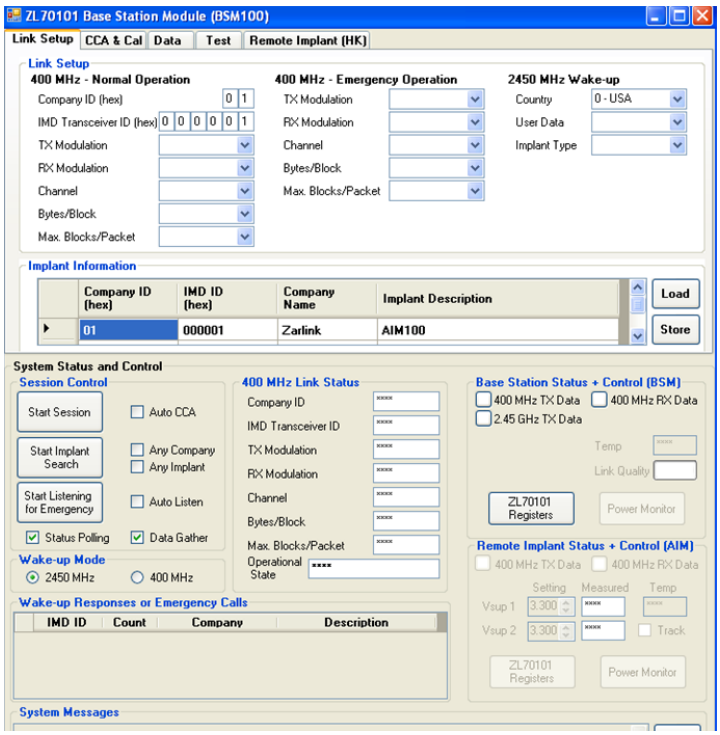

Figure 48 Base Station Module (BSM100) Main Form.

As shown in Figure 47, Base Station Module (BSM100) Main Form has following function tags:

- Link Setup: Setup connection and display link properties
- CCA & Cal: Perform Clear Channel Assessment (CCA) and calibration (CAL)
- Data: Send and receive data
- Test: Enable and disable carrier wave, set transmitter level
- Remote Implant: Not applicable now

The BSM100 main form for the ADK is divided into two main sections. The upper section is comprised of a tabular form that allows access to the different configuration settings of the ZL7010X as well as providing for control of operational modes of the device. The lower section if comprised of a static display that allows for basic system status and control for the main operational features of the ZL70101. The link can be set up by using “Start Session” or “Start listening to Emegency”.

B.2 Application Implant Module (AIM100) Main Form

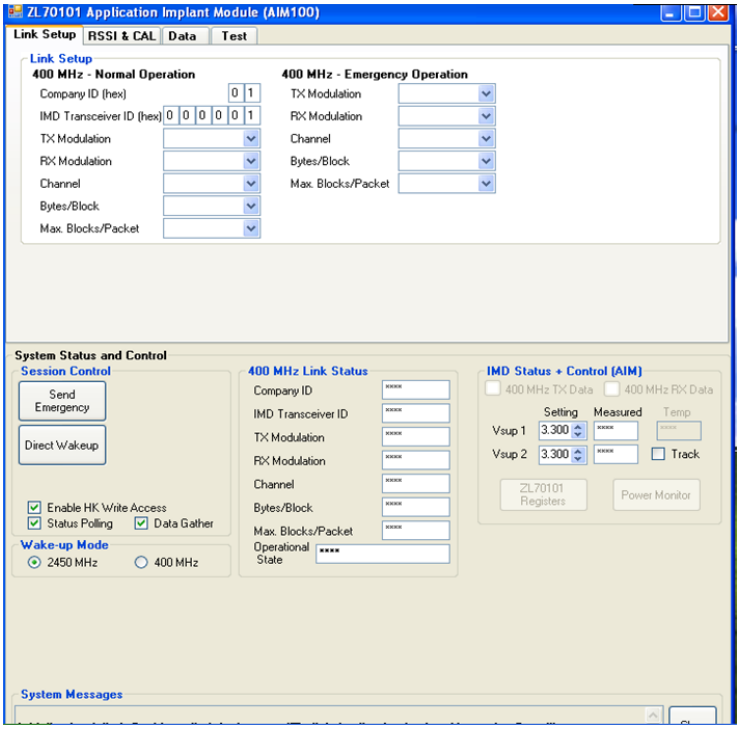

Figure 49 Application Implant Module (AIM100) Main.

As shown in Figure 49, The AIM100 main form for the ADK is also divided into two main sections. The upper section is comprised of a tabular form that allows access to the different configuration settings of the ZL70101 as well as providing for control of operational modes of the device. The lower section if comprised of a static display that allows for basic system status and control for the main operational features of the ZL70101. Alike Base Station Module Main Form, it has several function tags as well:

- Link Setup: Setup connection and display link properties
- RSSI & CAL: Reading RSSI and calibration (CAL)
- Data: Send and receive data
- Test: Enable and disable carrier wave, set transmitter level

The Application Implant Module can function as transmitter using “Send Emergency” or as receiver using “Direct Wakeup”. When the Base Station Module is trying to “Start Session”, Implant will react automatically without the need to “Direct Wakeup”.

3.1.2.4.3 Programming ZL70101 ADK Firmware

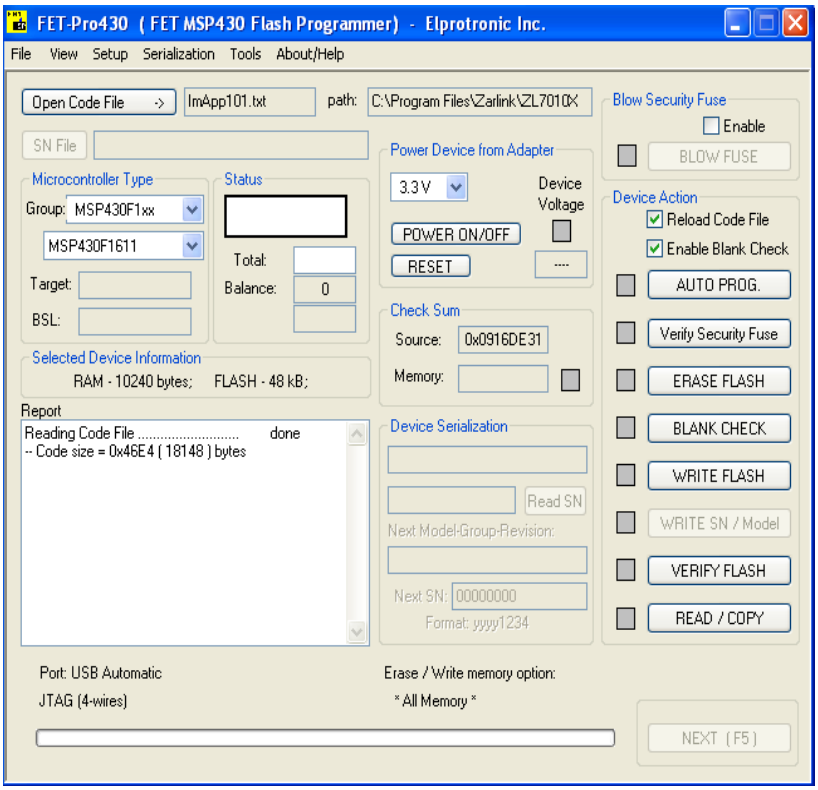

Figure 50 Programming ZL70101 ADK Firmware Elprotronic FET-Pro430

This software (Figure 50) helps to program the firmware on the boards included with the ZL70101 Application Development Kit.

To use the Elprotronic FET-Pro430, follow these steps:

- Connect the MSP-FET430UIF to the PC via USB.
- Connect the ADP board to the PC via USB

- Turn on the power switch on the ADP board, or if the power switch is already on, press the reset button on the ADP board.
- Under “Microcontroller Type”, select the MSP430F1611.
- Click “Open Code File” and browse to the firmware file for the target board.
    a) BsmApp101.txt (for the ZL70101 base station mezzanine board)
    b) BsmApp102.txt (for the ZL70102 base station mezzanine board)
    c) ImApp101.txt (for the ZL70101 implant mezzanine board)
    d) ImApp102.txt (for the ZL70102 implant mezzanine board)
    e) AdpApp.txt (for the ADP board)
- Under “Device Action”, check “Reload Code File”, click “AUTO PROG.”

This software tool is very useful when we need to reload the original Zarlink source code, especially when users modified code of Zarlink board in a wrong way and lose control of it. FET-Pro430 helps to reset all the default settings of Zarlink.

When performing “AUTO PROG” auto progress, it will check all the functions displays under that button (i.e. Verify Security Fuse etc.). If progress successful, a green indicator will appear, otherwise a red fork will appear. At the bottom of this software is the progress bar. When it finished we can remove Zarlink ADK boards from the JTAG connector.

3.1.2.4.5 ZL70101 ADK Programming Software

ZL70101 ADK has provided the software includes three main categories: Graphical User Interfaces (GUI's), Application Programming Interfaces (API's), and embedded software for the MSP430 boards (ADP board, base station mezzanine board, and implant mezzanine board).

Code Compose Studio v4 is used in our thesis as compiler and debugger. To start with Zarlink's Source Code, first starting CCE, and if it prompts you to select a workspace, browse to the workspace ZL70101 ADK has offered you. Then, be sure if it is the first time you start CCE for a new source tree, you must update the TOP variable in the CCE workspace for the source tree. To do so, open "Window, Preferences, General, Workspace, Linked Resources" in CCE and change TOP to point to the top directory of the source tree. Afterwards, refresh all of the projects in CCE so it will update its links. Now we can begin modifying the codes. The User Graphic Interface of CCS4 is as below:

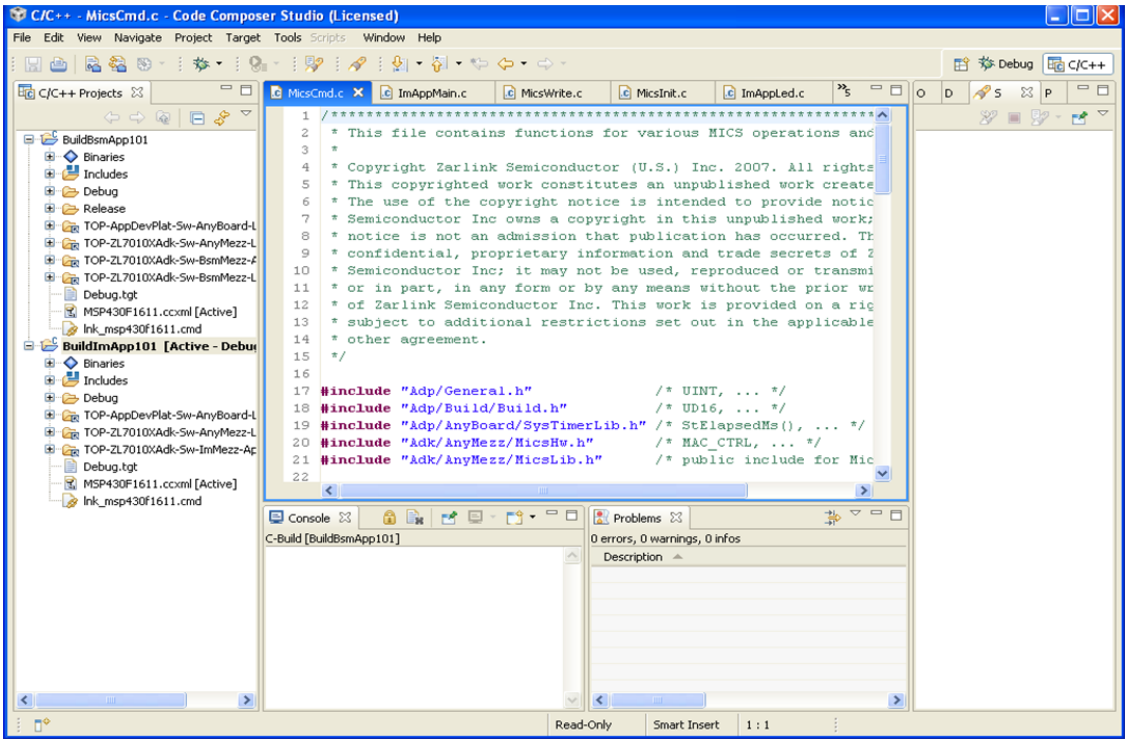

Figure 51 Code Composer Studio version 4 User Graphic

3.1.2.5 Other Subsidiary Software

Software named "HyperSnap 7" and "Button Wizard" is also used in this thesis. HyperSnap supports snapshot screen contents from user defined region and convert captured

images into word file. This is useful for recording Receive Signal Strength Indicator (RSSI) variation. “Button Wizard” is used to assist HyperSnap by writing and running a Script, imitating mouse movement and clicking to repeat snapshot action.

3.1.2.5 Other Subsidiary Hardware

Other hardware components such as Signal Generator, Spectrum Analyzer, Network Analyzer, Variable Attenuation, Power Splitter, Circulator, PC connecting with Zarlink Advanced Development Kit and several cables are used in this thesis.

Signal generator is used to support RF local input. Spectrum Analyzer is used to read receive signal strength, network analyzer is used to collect received signal and analyze fading properties. Variable attenuation is used to protect PROPSim and simulate distance change. Power splitter and circulator help to fulfill circuit functions.

References

[1] Sofia Najwa Ramli, Rabiah Ahmad, "Surveying the Wireless Body Area Network in the realm of Wireless Communication," in *Information Assurance and Security (IAS), 2011 7th International Conference*, 5-8, Dec, 2011.

[2] S. Drude, "Requirements and Application Scenarios for Body Area Networks," in *obile and Wireless Communications Summit, 2007. 16th IST*, 1-5, July 2007.

[3] Fabio Di Franco, Christos Tachtatzis, Ben Graham, Marek Bykowski, David C. Tracey, Nick F. Timmons et al., "The effect of body shape and gender on Wireless Body Area Network on-body channels," in *IEEE APS, Middle East Conference on Antennas and Propagation (MECAP)*, Cairo, Egypt, 2010.

[4] Emil Jovanov*, Aleksandar Milenkovic, Chris Otto and Piet C de Groen, "A wireless body area network of intelligent motion sensors for computer assisted physical rehabilitation," *Journal of NeuroEngineering and Rehabilitation,* vol. 2, no. 6, 2005.

[5] Marina Sukor, Sharifah Ariffin and Norsheila Fisal and S.K. Syed Yusof, Adel, "Performance Study of Wireless Body Area Network in Medical Environment," in *Modeling & Simulation, 2008. AICMS 08. Second Asia International Conference*, 13-15, May 2008.

[6] "Ansoft HFSS 3D full-wave electromagnetic field software datasheet," [Online]. Available:

http://www.ansoft.com/products/hf/hfss/datasheet.cfm?f=HFSS_Flysheet.pdf.

[7] Sergey N. Makarov, Umair I. Khan, Md. Monirul Islam, Reinhold Ludwig, Kaveh Pahlavan, "On Accuracy of Simple FDTD Models for the Simulation of Human Body Path Loss," in *Sensors Applications Symposium (SAS), 2011 IEEE*, San Antonio, TX, February 22-24, 2011.

[8] *PROPSim™ C8 Wideband Multichannel Simulator: Operational Manual, August 2002 Edition,* Elektrobit Group, Ltd. , August 2002.

[9] Metreaud, L.T., Pahlavan, K., "RF Isolated Real-Time Multipath Testbed for Performance Analysis of WLANs," in *Information Sciences and Systems, 2006 40th Annual Conference*, Princeton, NJ, 22-24 March 2006.

[10] M. P. K. Heidari, "Performance evaluation of indoor geolocation systems using PROPSim hardware and ray tracing software," in *Wireless Ad-Hoc Networks, 2004 International Workshop, IWWAN*, Oulu, Finland, June, 2004.

[11] M. Hassan-Ali, and K. Pahlavan, "Site-Specific Wideband and Narrowband Modeling of Indoor Radio Channel Using Ray-Tracing," in *IEEE PIMRC'98*, Boston, MA, September 8-11, 1998.

[12] Aung Aung Phyo Wai, Wei Ni, Robert Hsieh and Yu Ge, "Development of Visualization and Performance Evaluation Testbed for Wireless Body Area Network," in *e-Health Networking Applications and Services (Healthcom), 2011 13th IEEE International Conference*, 11-13, June 2011.

[13] L. T. Metreaud, "An RF-Isolated Real-Time Multipath Testbed for Performance Analysis of WLANs," ECE Department, WPI, Worcester, MA, 2006.

[14] M. Heidari, "A Test-bed for Real-time Performance Evaluation of Indoor Geolocation Systems in Laboratory Environment," 2005.

[15] M. A. Assad, "A REAL-TIME LABORATORY TESTBED FOR EVALUATING LOCALIZATION PERFORMANCE OF WIFI RFID TECHNOLOGIES," ECE Department, WPI, Worcester, MA, USA, May 4, 2007.

[16] Jie He, Shen Li, Qin Wang, Kaveh Pahlavan, "6th International Symposium on Medical Information and Communication Technology (ISMICT2012)," in *IEEE International Conference on Communications (ICC)*, Ottawa, Canada, 2012.

[17] E. A. Lee, "Cyber Physical Systems: Design Challenges," in *11th IEEE Symposium on Object Oriented Real-Time Distributed Computing (ISORC)*.

[18] Gill, Radhakisan Baheti and Helen, "Cyber-physical Systems," in *The Impact of Control Technology,T. Samad and A.M. Annaswamy (eds.)*, 2011.

[19] *NSF Workshop On Cyber-Physical Systems,* 06.09.2008.

[20] "NIST Foundations for Innovation in Cyber-Physical Systems Workshop," 02,08,2012.

[21] "NSF Cyber-Physical Systems Summit," 08,01,2008.

[22] Shen Li, Jie He, Ruijun Fu, Kaveh Pahlavan, "A Hardware Platform for Performance

Evaluation of In-body Sensors," in *6th International Symposium on Medical Information and Communication Technology (ISMICT2012)*, La Jolla, 2012.

[23] Jie He, Kaveh Pahlavan, Shen Li, Qin Wang, "A Testbed for Evaluation of the Effects of Multipath on Performance of TOA-based Indoor Geolocation," *IEEE transactions on instrumentation and measurement,* 2012.

[24] "Body Area Networks," [Online]. Available: http://en.wikipedia.org/wiki/Body_area_network.

[25] "Monitoring your health with your mobile phone," Imec, [Online]. Available: http://www.imec-nl.nl/nl_en/press/imec-news/wirelesshealthnecklaceinterface.html.

[26] Given Imaging, [Online]. Available: http://www.givenimaging.com/en-us/Pages/GivenWelcomePage.aspx.

[27] Li Yin-lin, Huang Zhong-hua , "Modeling of Body Area Network in medical healthcare applications," in *IT in Medicine & Education, 2009. ITIME '09. IEEE International Symposium*, 14-16 Aug. 2009.

[28] Muhammad Shuja Uddin, Noohul Basheer Zain Ali and Nor Hisham Hamid, "Wave propagation and energy model for dynamic Wireless Body Area Networks," in *Electrical, Control and Computer Engineering (INECCE), 2011 International Conference*, 21-22 June 2011.

[29] Sang-Hun Han and Sang Kyu Park, "Performance analysis of wireless body area network in indoor off-body communication," *Consumer Electronics, IEEE Transactions,*

Vols. 57 , Issue: 2 , pp. 335-338, May 2011.

[30] Puduru Viswanadha Reddy, Viswanath Ganapathy, "Performance of multi user detector based receivers for UWB body area networks," in *-health Networking, Applications and Services, 2008. HealthCom 2008. 10th International Conference*, 7-9 July 2008.

[31] Raúl Chávez-Santiago1,2, Ali Khaleghi1,2, Ilangko Balasingham1,2 and Tor A. Ramstad2, "Architecture of an ultra wideband wireless body area network for medical applications," in *Applied Sciences in Biomedical and Communication Technologies, 2009. ISABEL 2009. 2nd International Symposium*, 24-27 Nov. 2009.

[32] F. R. a. Regulations, *MICS Band Plan, Part 95,* Jan. 2003.

[33] Kazunari Tai, Hiroki Harada, Ryuji Kohno, "Channel Modeling and Signaling of Medical Implanted Communication Systems and a Step to Medical ICT," in *16thIST Mobile & wireless communication, Special session on medical ICT*, June 1-4, 2007.

[34] Sean F. Heaney, William G. Scanlon, E. Garcia-Palacios, Simon L. Cotton, "Fading characterization for Context Aware Body Area Networks (CABAN) in interactive smart environments," in *Antennas and Propagation Conference (LAPC), 2010 Loughborough*, 8-9 Nov. 2010.

[35] Kamran Sayrafian-Pour, Wen-Bin Yang, John and Kamya Yekeh Yazdandoost, "A Statistical Path Loss Model for Medical Implant Communication Channels," in *PIMRC, IEEE 20th International Symposium*, Tokyo Japan, 2009.

[36] *ZL7010X Application Development Kit User's Guide, Version 2.0.0,* Zarlink , March 19, 2009.

[37] Xinghong Kuang, Huihe Shao, "Maximum Likelihood Localization Algorithm Using Wireless Sensor Networks," in *Innovative Computing, Information and Control, 2006. ICICIC '06. First International Conference*, Aug. 30 2006-Sept. 1 2006.

[38] H. Cramér, Mathematical Methods of Statistics., Princeton, NJ: Princeton Univ. Press. ISBN 0-691-08004-6. OCLC 185436716.

[39] Jie He, Qin Wang, Qianxiong Zhang, Bingfeng Liu and Yanwei Yu, "A practical indoor TOA ranging error model for," in *IEEE 22nd International Symposium on Personal, Indoor and Mobile Radio Communications*, 2011.

[40] Jie He, Shen Li, Qin Wang, Kaveh Pahlavan, "A Testbed for Evaluation of the Effects of Multipath on Performance of TOA-based Indoor Geolocation".